The Time-Freezing Reformulation for Numerical Optimal Control of Complementarity Lagrangian Systems with State Jumps

Armin Nurkanović, Sebastian Albrecht, Bernard Brogliato, Moritz Diehl

The Time-Freezing Reformulation for Numerical Optimal Control of Complementarity Lagrangian Systems with State Jumps. ⋆

Armin Nurkanović [a], Sebastian Albrecht [c], Bernard Brogliato [d], Moritz Diehl [a,b],

[a] *Department of Microsystems Engineering (IMTEK), University of Freiburg, Germany*

[b] *Department of Mathematics, University of Freiburg, Germany*

[c] *Siemens Technology, Munich, Germany*

[d] *Univ. Grenoble Alpes, INRIA, CNRS, Grenoble INP, LJK, Grenoble, France*

Abstract

This paper introduces a novel reformulation and numerical methods for optimal control of complementarity Lagrangian systems with state jumps. The solutions of the reformulated system have jump discontinuities in the first time derivative instead of the trajectory itself, which is easier to handle theoretically and numerically. We cover not only the easier case of elastic impacts, but also the difficult case, when after the state jump the system evolves on the boundary of the dynamic's feasible set. In nonsmooth mechanics this corresponds to inelastic impacts. The main idea of the time-freezing reformulation is to introduce a clock state and an auxiliary dynamic system whose trajectory endpoints satisfy the state jump law. When the auxiliary system is active, the clock state is not evolving, hence by taking only the parts of the trajectory when the clock state was active, we can recover the original solution. We detail how to recover the solution of the original system, show how to select appropriate auxiliary dynamics and give practical numerical methods to handle discontinuous ODEs with nonunique sliding motions. Moreover, we introduce a novel auxiliary ODE for time-freezing for elastic impacts and overcome some drawbacks of [22]. The theoretical findings are illustrated on the nontrivial numerical optimal control example of a hopping one-legged robot.

Key words: non-smooth and discontinuous problems, modeling for control optimization, numerical algorithms, algorithms and software, parametric optimization

1 Introduction

Many real-word physical occurrences experience structural changes depending on their state (e.g., electric circuits with diodes) or comprise phenomena with largely different time-scales (e.g., mechanical impacts). Mathematically, these occurrences can readily be modeled via nonsmooth differential equations. This paper is concerned with numerical methods for Optimal Control Problems (OCP) with some classes of such dynamic systems. For an overview of different mathematical formalism for nonsmooth Ordinary Differential Equations (ODEs) the reader is referred to [1,9,28].

The solution trajectories of the systems of interest are usually smooth pieces joined by kinks and jumps. Hence, the discontinuities arise either in the trajectory itself or its time derivatives. This leads to one possible classification which covers numerous, but not all mathematical formalisms for nonsmooth ODEs. It regards continuity of the state trajectory $x(t; x_0)$ and its time derivatives. We distinguish NonSmooth Dynamics (NSD) with the following properties:

(NSD1) continuous, but nonsmooth r.h.s., jump discontinuity in the 2[nd] time derivative - $\mathcal{C}^1$ solutions, e.g., $\dot{x} = |x|$,

⋆ This research was supported by the German Federal Ministry of Education and Research (BMBF) via the funded Kopernikus project: SynErgie (03SFK3U0), DFG via Research Unit FOR 2401 and project 424107692 and by the EU via ELO-X 953348. Corresponding author A. Nurkanović.
Email address: armin.nurkanovic@imtek.uni-freiburg.de (Armin Nurkanović), sebastian.albrecht@siemens.com (Sebastian Albrecht), bernard.brogliato@inria.fr (Bernard Brogliato), moritz.diehl@imtek.uni-freiburg.de (Moritz Diehl)

(NSD2) discontinuous r.h.s., jump discontinuity in the first time derivative - absolutely continuous (AC) solutions, e.g., $\dot{x} \in -\text{sign}(x)$,

(NSD3) jump discontinuity in the trajectory - solutions are functions of bounded variation (BV), e.g., $\ddot{x} \in f(x) - \mathcal{N}_{\mathbb{R}^+}(x)$.

State jumps appear commonly if the dynamics are constrained by an inequality. When the trajectory reaches the boundary of the feasible set transversally, in order to stay feasible a state jump in the velocities must occur. There are two possible outcomes: either the evolution continues in the strict interior of the feasible set or on its boundary. The outcome is determined by a pointwise *state jump law* or *restitution law*. The former are denoted as systems with *(partially) elastic impacts* and the latter systems with *inelastic impacts*.

Since systems with state jumps are difficult to treat numerically and theoretically within optimal control problems, a natural question is: can we transform them into simpler systems? In the literature we can find affirmative answers, but often at the cost of several drawbacks and severe inaccuracies. Common approaches are either to use coordinate transformations [17,32] or to use penalization/smoothing [29,30] and compliant contact models [8, Chapter 2]. The former have the advantage that they are exact, i.e., we can recover the solution of the original system. But they are usually limited to special cases, namely partially elastic impacts and a single scalar constraint. Examples are the Zhuravlev-Ivanonv transformation [32],[8, Sec 1.4.3.] and the gluing function approach [17] in the hybrid systems formalism. In [22] we have introduced an exact transformation of problems from case NSD3 with (partially) elastic impacts into case NSD2. In this article we extend these ideas to the inelastic case for Complementarity Lagrangian Systems (CLS). The relevant tasks of locomotion, jumping, grasping and manipulation in robotics require inelastic impacts.

1.1 Contributions

This paper introduces a reformulation of complementarity Lagrangian systems (NSD3) with a unilateral constraint into a ODE with an discontinuous r.h.s. (NSD2). The latter class is in general easier, and poses a rich theoretical and computational toolkit which we aim to exploit. We discuss how to select auxiliary dynamics and formalize the relationship between the time-freezing Piecewise Smooth Systems (PSS) and CLS. Thereby, we provide a constructive way to recover the solution of the original system. In addition, we introduce a novel auxiliary ODE for elastic impacts which enables to treat nonlinear constraints and multiple impacts, which was not possible in [22]. The time-freezing PSS may have nonunique sliding motions on manifolds of higher codimensions. We provide practical methods for solving OCPs with such systems and propose an approach that enables one to select a desired sliding motion even if the solution is not unique in general. Furthermore, we introduce an extension for state jumps in tangential directions due to friction. The theoretical considerations and efficacy of the proposed numerical methods are demonstrated on the challenging OCP example where the dynamic trajectory of a hopping robot is computed, which has to reach a certain goal while jumping over holes. Our numerical OCP strategy relies on solving mathematical programs with complementarity constraints with a homotopy approach. Thereby, we solve only a few smooth NLPs and recover the highly nonsmooth solutions with state jumps.

1.2 Outline

The remainder of this paper is structured as follows. In Section 2 the main ideas are depicted on an illustrative example. Section 3 give an introduction to PSS, their embedding into Filippov's framework, DCS and how PSS can be transformed into DCSs. This is followed by Section 4 where the time-freezing reformulation is discussed in detail. Section 5 discusses computational issues and introduces practical methods for optimal control of time-freezing systems. In Section 6 we discuss extensions regarding frictional impacts. Section 7 provides a numerical example of using time-freezing in a robotics optimal control problem. We conclude and list some future research directions in Section 8.

1.3 Notation

For the left and the right limits we use the notation $x(t_\text{s}^+) = \lim_{t \to t_\text{s},\ t > t_\text{s}} x(t)$ and $x(t_\text{s}^-) = \lim_{t \to t_\text{s},\ t < t_\text{s}} x(t)$, respectively. Time derivatives of a function $x(t)$ w.r.t. to t are compactly denoted as $\dot{x}(t) \coloneqq \frac{\mathrm{d}x(t)}{\mathrm{d}t}$, and of a function $y(\tau)$ w.r.t. to τ as $y'(\tau) \coloneqq \frac{\mathrm{d}y(\tau)}{\mathrm{d}\tau}$. For ease of notation, when clear from the context we drop the t ,τ or x-dependencies. All vector inequalities are to be understood element-wise. The complementary conditions for two vectors $a, b \in \mathbb{R}^n$ read as $0 \leq a \perp b \geq 0$, where $a \perp b$ means $a^\top b = 0$, The matrix $\mathbf{1}_{n,n} \in \mathbb{R}^{n \times n}$ is the identity matrix, and $\mathbf{0}_{m,n} \in \mathbb{R}^{m \times n}$ is the zero matrix. The concatenation of two column vectors $a \in \mathbb{R}^m$, $b \in \mathbb{R}^n$ is denoted as $(a, b) \coloneqq [a^\top, b^\top]^\top$. The concatenation of several column vectors is defined in a analogous way. A vector with all ones is denoted as $e_k = (1, 1, \ldots, 1) \in \mathbb{R}^k$. The closure of a set X is denoted as $\overline{X}$, its boundary as ∂X and $\text{conv}(X)$ is its convex hull. With $\mu(\cdot)$ we denote the Lebesgue measure. Suppose $f : \mathbb{R}^n \to \mathbb{R}^m$ is a single-valued and $F : \mathbb{R}^n \rightrightarrows \mathbb{R}^m$ a set-valued mapping, then we call the inclusion $f(x) + F(x) \ni 0$ a *generalized equation*. In this paper $F(x)$ is usually the normal cone over a convex set C: $\mathcal{N}_C(x) \coloneqq \{y \in \mathbb{R}^n \mid y^\top (y' - x) \leq 0, \forall y' \in C\}$. The tangent cone of a set Ω at $x \in \Omega$ is defined as the set $\mathcal{T}_\Omega(x) \coloneqq \left\{ \lim_{i \to \infty} \frac{x_i - x}{t_i} \mid x_i \in \Omega,\ t_i \to 0 \text{ as } i \to \infty \right\}$. The set $B(x) \coloneqq \{y \mid \|y - x\| \leq 1\}$ denotes the unit Euclidean ball centered at x.

2 An Illustrative Example

This section introduces the main ideas behind the time-freezing reformulation on a simple example. The latter sections will generalize and formalize all ideas in more detail.

Example 1 *Consider a frictionless point-mass in two dimensions above a horizontal table. The mass is* $m = 1$ kg *and let* g *be the gravitational acceleration. Denote with* $q(t) := (q_x(t), q_y(t))$ *and* $v(t) := (v_x(t), v_y(t))$ *its position and velocity, respectively, and let* $z(t)$ *be the normal contact force. The dynamics are given by the CLS:*

$$m\dot{v}(t) = \begin{bmatrix} 0 \\ -mg \end{bmatrix} + \begin{bmatrix} 0 \\ 1 \end{bmatrix} z(t), \ \dot{q}(t) = v(t), \tag{1a}$$

$$0 \leq z(t) \perp q_y(t) \geq 0, \tag{1b}$$

$$v_y(t_s^+) = -\epsilon v_y(t_s^-), \text{ if } q_y(t_s) = 0 \text{ and } v_y(t_s^-) < 0. \tag{1c}$$

The complementarity condition (1b) states: the point-mass is either not in contact ($q_y > 0$) and there is no reaction force $z = 0$, or there is contact ($q_y = 0$) and a reaction force ($z \geq 0$). If the particle hits the table ($q_y(t_s) = 0$) with a negative normal velocity ($v_y(t_s^-) < 0$), then the normal velocity must jump to a positive value (elastic impacts) or become zero (inelastic impacts) in order to meet the constraint $q_y \geq 0$. Equation (1c) is the point-wise *state jump law*, with $\epsilon \in [0, 1]$, which determines the velocity after an impact. The fact that jump discontinuities are state dependent, i.e., happen at time points that are a-priori unknown, makes their treatment in numerical optimal control notoriously difficult.

2.1 Main Ideas

The *time-freezing reformulation* transforms dynamic systems with state jumps (NSD3), such as the one from Example 1, into piecewise smooth systems (NSD2), where no state jumps are present. It builds upon three main ideas. First, it mimics the state jump with an *auxiliary dynamic system* $\dot{x} = \psi(x)$ in the *infeasible* region (in the example $q_y < 0$). The trajectory endpoints of the auxiliary ODE satisfy the state jump law on some finite time interval. Second, introduce a *clock state* $t(\tau)$ that stops counting when the auxiliary system is active, i.e., $t'(\tau) = 0$. Third, in optimal control problems, adapt the speed of time $\frac{\mathrm{d}t}{\mathrm{d}\tau} = s$ with $s \geq 1$, and impose terminal constraint $t(T) = T$ in order to catch up for the additional time needed by the auxiliary ODE. In pure simulations problems we have $s = 1$ and no terminal constraints. Consequently, by taking the pieces of the trajectory when the clock state was active, one can recover the solution of the original system with discontinuous trajectories. The time of the time-freezing system τ is called *numerical time*. The intervals with $t'(\tau) = 1$ are referred to as *physical time* and those with $t'(\tau) = 0$ as *virtual time*. Partially elastic and inelastic impacts require a slightly different treatment.

2.2 Elastic Impacts

For partially elastic impact we have $\epsilon \in (0, 1]$, which means the post-impact velocity is positive, hence the particle does not stay on the table, but bounces back. The time-freezing reformulation for this case was introduced in [22]. For $c(x) := q_y > 0$ we have an evolution according to an ODE denoted compactly as $\dot{x} = f(x)$, with $z = 0$ (free flight). When q_y becomes zero, then $z > 0$ is a Dirac impulse ensuring that $v_x(t_s^+) = -\epsilon v_x(t_s^-)$ holds. In time-freezing, the role of the Dirac impulse, which causes instantaneous velocity changes, is taken by the auxiliary ODE $\dot{x} = \psi(x)$. The time-freezing system has the augmented state $(x, t) \in \mathbb{R}^{n+1}$ which evolves in numerical time τ and reads as

$$\frac{\mathrm{d}}{\mathrm{d}\tau} \begin{bmatrix} x \\ t \end{bmatrix} = \begin{cases} s \begin{bmatrix} f(x) \\ 1 \end{bmatrix}, & \text{if } c(x) \geq 0 \\ \\ s \begin{bmatrix} \psi(x) \\ 0 \end{bmatrix}, & \text{if } c(x) < 0. \end{cases} \tag{2}$$

An example phase plot for the relevant parts of the state space (the vertical position and normal velocity) is depicted in Figure 1 (left plot). The blue (dashed) and green (solid) curves together are a solution trajectory of the *time-freezing system*. The blue curve in the red (shaded) area ($q_y < 0$) is the trajectory of the auxiliary ODE. During this period the time is frozen, cf. Figure 1 (bottom left plot). By plotting the states as function of the physical time ($t'(\tau) = 1$) we recover the solution of the initial system (green solid curve).

2.3 Inelastic Impacts

Inelastic impacts with $\epsilon = 0$ are slightly more difficult to treat. In this case, when the particle hits the table, it stays on it, i.e., it evolves in a lower dimensional subspace. In our example, the system evolves according to a Differential Algebraic Equation (DAE) of index 3:

$$\begin{aligned} m\dot{v}(t) &= \begin{bmatrix} 0 \\ -mg \end{bmatrix} + \begin{bmatrix} 0 \\ 1 \end{bmatrix} z(t), \ \dot{q}(t) = v(t), \\ 0 &= q_y(t). \end{aligned}$$

An example phase plot is depicted in Figure 1, top right. Again, the blue (dashed) curves correspond to the evolution of the auxiliary ODE, and the green (solid) to the initial system with state jumps. Together they provide a continuous function in time (no state jumps anymore). By plotting only the parts when the time was running

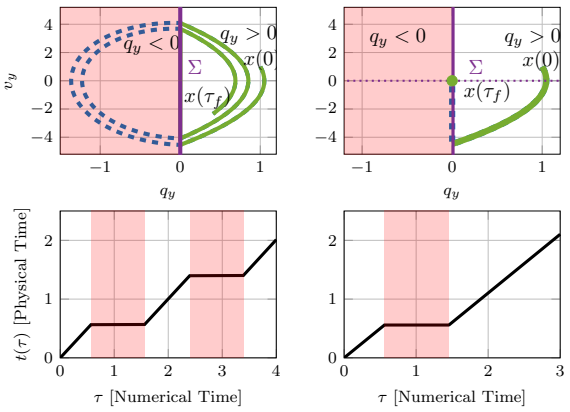

Fig. 1. Illustration of phase plots (top) and the clock states with speed of time $s = 1$ (bottom) for the time-freezing reformulation for an elastic impact (left) and an inelastic impact (right).

(green solid curve) one can recover the original solution. In this example the time-evolution after the state jump continues in the x-direction according to the DAE above (the particle slides on the table). This is depicted with the green dot at the origin. From a PSS point of view this is a *sliding motion*. ODEs for siding motions on some manifold (here the origin) are usually defined by the neighboring vector fields (cf. Subsection 3.2). One has to ensure that the sliding mode matches the DAE after the impact. To achieve this, besides the auxiliary ODE, we define additionally a *DAE-forming ODE* in the *infeasible* region, which deliverers the necessary ingredients to ensure the equivalence. This is discussed in detail in Section 4.

3 Nonsmooth Differential Equations

In this section we focus on DCS, PSS and their embedding into Filippov's framework [13]. In our study, the former are computationally convenient for discretization, the latter we found useful for modeling and a theoretical analysis.

3.1 Dynamic Complementarity Systems

Definition 2 (Dynamic Complementarity System) *A dynamic complementarity system is defined by:*

$$\dot{x}(t) = f_{\mathrm{DCS}}(x(t), z(t)), \tag{3a}$$
$$0 \le z(t) \perp g_{\mathrm{DCS}}(x(t), z(t)) \ge 0, \tag{3b}$$

where $x \in \mathbb{R}^{n_x}$, $z \in \mathbb{R}^{n_z}$. The functions $f_{\mathrm{DCS}} : \mathbb{R}^{n_x} \times \mathbb{R}^{n_z} \to \mathbb{R}^{n_x}$ and $g_{\mathrm{DCS}} : \mathbb{R}^{n_x} \times \mathbb{R}^{n_z} \to \mathbb{R}^{n_z}$ are assumed to be smooth.

The relative degree r between the complementarity variables $z(t)$ and $w(t) \coloneqq g_{\mathrm{DCS}}(x(t), z(t))$ is defined as the number of times $w(t)$ has to be differentiated w.r.t. t until $z(t)$ appears explicitly. The smoothness of the DCS solution depend strongly on it. For example; systems with $r = 2$ have usually state jumps (NSD3), and systems with $r = 1$ have AC solutions (NSD2) [9]. The definition of DCS with $r = 2$ is additionally equipped with state jump laws. More details are provided in the next section.

3.2 Piecewise-Smooth Systems

We consider discontinuous ODEs (case NSD2) with the following structure.

Definition 3 (Piecewise-Smooth Systems) *A PSS is defined by a finite set of ODEs:*

$$\dot{x}(t) = f(x(t)), \text{ with } f(x) = f_i(x), \quad \text{if } x \in R_i \subset \mathbb{R}^{n_x},\ i \in \mathcal{I} \coloneqq \{1, \dots, N_{\mathrm{S}}\}, \tag{4}$$

where the functions $f_i \in \mathcal{C}^\infty(\overline{R_i}, \mathbb{R}^{n_x})$ define systems on the disjoint, connected and open regions R_i, $i \in \mathcal{I}$. Denote by $R \coloneqq \cup_{i=1}^{N_{\mathrm{S}}} R_i$ and $\partial R \coloneqq \cup_{i=1}^{N_{\mathrm{S}}} \partial R_i$, the combined regions and boundaries, respectively. Their closure is assumed to cover $\mathbb{R}^n$, i.e., $\mathbb{R}^n = \overline{R}$ and $\mu(\mathbb{R}^n \setminus R) = 0$.

The regions R_i are assumed to have a nonempty interior and piecewise-smooth boundaries ∂R_i. The ODE (4) is not properly defined on the boundary ∂R and a solution trajectory $x(t; x_0)$ of (4) might need to evolve on ∂R_i for some initial value x_0. Trajectories evolving on ∂R are called *sliding motions* [13]. One needs to make a modeling decision and choose how to define the dynamics on ∂R. The most widely used approach is to embed the PSS from Definition 3 into Filippov's framework, where the main idea is to replace the r.h.s. of (4) with a convex set and to obtain the following Differential Inclusion (DI):

$$\dot{x}(t) \in F_{\mathrm{F}}(x(t)), \tag{5a}$$
$$F_{\mathrm{F}}(x) \coloneqq \bigcap_{\delta>0} \bigcap_{\mu(N)=0} \overline{\mathrm{conv}} f(x + \delta B(x) \setminus N). \tag{5b}$$

Loosely speaking, $F_{\mathrm{F}}(x)$ is the convex hull of values of the vector field nearby, ignoring the values on null sets N, i.e., ∂R. For sufficient conditions for existence and uniqueness of solutions cf. [13]. On ∂R the set $F_{\mathrm{F}}(x)$ is in general not a singleton [12,13] and for computational considerations we might be interested to pick one element. We call a chosen element of $F_{\mathrm{F}}(x)$ a *selection* and denote it as $\hat{f}_{\mathrm{F}}(x) \in F_{\mathrm{F}}(x)$.

3.2.1 Relating PSS to DCS

Our next goal is to discuss the link between PSS, their embeddings and DCS, since this will be helpful for developing practical numerical methods. For ease of notation we focus on the case where we have only four

regions, i.e., $N_\mathrm{S} = 4$. Assuming that the sets R_i are separated by implicitly defined smooth manifolds of codimension 1, namely $\Sigma_1 = \{x \in \mathbb{R}^{n_x} \mid h_1(x) = 0\}$ and $\Sigma_2 = \{x \in \mathbb{R}^{n_x} \mid h_2(x) = 0\}$, we label the regions w.l.o.g. as: $R_1 = \{x \mid h_1(x) < 0,\ h_2(x) < 0\}$, $R_2 = \{x \mid h_1(x) < 0,\ h_2(x) > 0\}$, $R_3 = \{x \mid h_1(x) > 0,\ h_2(x) < 0\}$ and $R_4 = \{x \mid h_1(x) > 0,\ h_2(x) > 0\}$. A very popular approach to rewrite PSS is to use set-valued step functions to determine which region is active [1,3,12,19]. The set-valued step function $\theta : \mathbb{R} \rightrightarrows \mathbb{R}$ is defined as

$$\theta(x) = \begin{cases} \{1\}, & x > 0, \\ [0,1], & x = 0, \\ \{0\}, & x < 0. \end{cases} \tag{6}$$

This function can also be expressed as the solution map of the parametric linear program [7]:

$$\theta(x) = \arg\min_{w} \ -xw \quad \text{s.t.} \quad 0 \le w \le 1. \tag{7}$$

The system (4) with $N_\mathrm{S} = 4$ can be rewritten as

$$\begin{aligned} \dot{x}(t) \in F_\mathrm{AP}(x) \coloneqq \Big\{ & (1-\alpha)(1-\beta) f_1(x) + (1-\alpha)\beta f_2(x) \\ & + \alpha(1-\beta) f_3(x) + \alpha\beta f_4(x) \mid \alpha \in \theta(h_1(x)), \\ & \beta \in \theta(h_2(x)) \Big\}. \end{aligned} \tag{8}$$

It is important to notice that the set $F_\mathrm{AP}(x)$ is not equal to $F_\mathrm{F}(x)$ in (5b), but is in general a strict subset of it [3]. The DI (8) is a so-called *Aizerman–Pyatnitskii* (AP) extension of the PSS (4), see [3, Definition 8] and [13, Definition c, page 55]. Similar to the previous section we denote a selection of the AP-extension as $\hat{f}_\mathrm{AP}(x) \in F_\mathrm{AP}(x) \subseteq F_\mathrm{F}(x)$. Using the KKT conditions of the parametric LP representation of $\theta(.)$ (7) we can recast (8) into a DCS, with $r = 1$.

4 The Time-Freezing Reformulation

As the elastic impact case was already treated in [22], we focus here on the more difficult case of inelastic impacts. In the Subsections 4.1 to 4.4 we introduce the time-freezing reformulation which enables us to transform a CLS with inelastic impacts (case NSD3) into a PSS (case NSD2). Moreover, since the auxiliary ODE for elastic impacts introduced in [22] has some drawbacks, we propose an extension in Subsection 4.5 which resolves these issues.

4.1 Complementarity Lagrangian Systems with Inelastic Impacts

In this paper, due to page limitations, we restrict our attention to $m = 1$, i.e., we have a single unilateral constraint for the dynamics. Extensions for multiple constrains and simultaneous impacts, based on the same main ideas, will be provided in a forthcoming paper. The CLS of interest is defined as follows.

Definition 4 (CLS with inelastic impacts) *A complementarity Lagrangian system with inelastic impacts is the DCS defined by:*

$$\dot{v}(t) = f_\mathrm{v}(q(t), v(t)) + G(q(t)) n(q(t)) z(t), \tag{9a}$$
$$\dot{q}(t) = v(t), \tag{9b}$$
$$0 \le z(t) \perp c(q(t)) \ge 0, \tag{9c}$$
$$\begin{aligned} & 0 = n(q(t_\mathrm{s}))^\top v(t_\mathrm{s}^+), \\ & \quad \text{if } c(q(t_\mathrm{s})) = 0 \text{ and } n(q(t_\mathrm{s}))^\top v(t_\mathrm{s}^-) < 0, \end{aligned} \tag{9d}$$

where $n(q(t)) \coloneqq \nabla_q c(q(t))$, with $q, v \in \mathbb{R}^{n_q}$ and $x \coloneqq (q, v) \in \mathbb{R}^{n_x}$ being the differential states and $z \in \mathbb{R}^m$ the algebraic states. The functions $f_\mathrm{v} : \mathbb{R}^{n_q} \times \mathbb{R}^{n_q} \to \mathbb{R}^{n_q}$, $G : \mathbb{R}^{n_q} \to \mathbb{R}^{n_q \times n_q}$, $c : \mathbb{R}^{n_q} \to \mathbb{R}^m$ are assumed to be at least twice continuously differentiable and the matrix $G(q)$ is assumed to be symmetric positive definite.

We denote an active-set change from $z(t_\mathrm{s}^-) = 0, c(q(t_\mathrm{s}^-)) \ge 0$ to $z(t_\mathrm{s}^+) \ge 0,\ c(q(t_\mathrm{s}^+)) = 0$ (which triggers a state jump) as an *impact*. Note that $c(q(t))$ needs to be differentiated two times until $z(t)$ appears explicitly, hence $r = 2$. For the DCS (9) we can distinguish two modes of operation: (i) the manifold is not reached, i.e., $c(q(t)) > 0$ which implies $z(t) = 0$, (ii) the manifold is reached, i.e., $c(q) = 0$ and $z(t) \ge 0$. In the former case the system evolves according to the ODE:

$$\dot{v}(t) = f_\mathrm{v}(q(t), v(t)),\ \dot{q}(t) = v(t). \tag{10}$$

We denote the r.h.s. compactly by $f_\mathrm{ODE}(x) = (v, f_\mathrm{v}(q, v))$. After an impact we have $0 = n(q(t_\mathrm{s}))^\top v(t_\mathrm{s}^+)$. Subsequently, the system evolves according to a DAE of index 3:

$$\dot{v}(t) = f_\mathrm{v}(q(t), v(t)) + G(q(t)) \nabla_q c(q(t)) z(t), \tag{11a}$$
$$\dot{q}(t) = v(t), \tag{11b}$$
$$0 = c(q(t)). \tag{11c}$$

The next question to be answered is: will the system stay in contact (dynamics defined by (11) with $c(q(t)) = 0$) or will the *contact break* (dynamics defined by (10) with $c(q) > 0$)? The answers can be found by looking at the *contact Linear Complementarity Problem* (LCP) [8, Section 5.1.2]. Under the conditions of Definition 4, during contact on some time interval $[t_1, t_2]$ the *consistent initialization* conditions hold

$$0 = c(q(t)),\ 0 = \frac{\mathrm{d}}{\mathrm{d}t} c(q(t)) = \nabla_q c(q(t))^\top v(t). \tag{12}$$

Consequently, $z(t) \ge 0, t \in [t_1, t_2]$. Due to continuity of $q(t)$, $c(q(t))$ and $\frac{\mathrm{d}}{\mathrm{d}t} c(q(t))$, for contact breaking (i.e.,

$c(q) = 0$ becoming inactive) it is required that $\ddot{c}(q) \geq 0$ for $[t_2, t_2 + \hat{\epsilon})$, for some $\hat{\epsilon} > 0$. Therefore, from (9c) we deduce that

$$0 \leq \frac{\mathrm{d}^2}{\mathrm{d}t^2} c(q(t)) \perp z(t) \geq 0. \tag{13}$$

Then, by computing $\frac{\mathrm{d}^2}{\mathrm{d}t^2} c(q(t))$ and using the r.h.s. of (11a), we obtain the contact LCP in $z(t)$:

$$0 \leq D(q)z(t) + \varphi(x) \perp z(t) \geq 0, \tag{14}$$

where $D(q) \coloneqq \nabla_q c(q)^\top G(q) \nabla_q c(q) \succ 0$ is the Delassus' matrix [8] and $\varphi(x) \coloneqq \nabla_q c(q)^\top f_\mathrm{v}(q, v) + \nabla_q (\nabla_q c(q)^\top v)$. The solution map of the LCP (14) is given by

$$z(t) = \max(0, -D(q)^{-1} \varphi(x)). \tag{15}$$

From the last equation we deduce that contact breaking or sticking depends on the sign of the function $\varphi(x)$. In the first case, $\varphi(x) \leq 0$ implies $z(t) \geq 0$ and $\ddot{c}(q) = 0$ due to (14). Therefore we have a persistent contact and the system evolves according to the DAE (11). Or equivalently, since (12) holds via index reduction and using (15), we can derive

$$z(t) = f_z(x) \coloneqq -D(q)^{-1} \varphi(x), \tag{16a}$$
$$f_{\mathrm{DAE,v}}(x) \coloneqq f_\mathrm{v}(x, v) + \; G(q) \nabla_q c(q) f_z(x), \tag{16b}$$

and obtain the ODE $\dot{x} = f_\mathrm{DAE}(x) \coloneqq (v, f_{\mathrm{DAE,v}}(x))$, which has the same solution as (11). In the second case, $\varphi(x) > 0$ implies $z(t) = 0$ and $\ddot{c}(q) > 0$, therefore the contact breaks and the system evolves according to the ODE (10). To summarize, if we switch from $f_\mathrm{ODE}(x)$ to $f_\mathrm{DAE}(x)$ a state jump must occur. Now the system evolves on the boundary of the feasible set according to the DAE (11), or equivalently according the ODE defined by $f_\mathrm{DAE}(x)$. On the other hand, if we switch from $f_\mathrm{DAE}(x)$ to $f_\mathrm{ODE}(x)$, we have a continuous transition without state jumps, i.e., *contact breaking* occurs.

4.2 Main Observations and Auxiliary Dynamics

The analysis above reveals that CLS with $r = 2$ have switches between ODEs and DAEs of index 3. This has already a flavor of a PSS, but the main obstacle to complete this transition are the state jumps. Large parts of the state space, namely $c(q) < 0$, are prohibited for the solution trajectories. Within time-freezing, we relax the constraint, i.e., allow $c(q) < 0$, and define an auxiliary ODE which mimics the state jump law (9d). Moreover, we introduce a clock state t evolving according to $t'(\tau) = 1$, when $c(q) > 0$. Whenever the auxiliary ODE is active, the clock state is not evolving, i.e., $t'(\tau) = 0$. For notational convenience, all states from Definition 4 in numerical time are equipped with a tilde, e.g., $\tilde{x}(\tau)$. The properties of the auxiliary dynamics are summarized in the next definition.

Definition 5 (Auxiliary Dynamics) *An auxiliary dynamic system $\tilde{x}'(\tau) = f_{\mathrm{A,n}}(\tilde{x}(\tau))$ has for every initial value $\tilde{x}(\tau_\mathrm{s}) = \tilde{x}_\mathrm{s} = (\tilde{q}_\mathrm{s}, \tilde{v}_\mathrm{s})$ with $c(\tilde{q}_\mathrm{s}) = 0$, $n(\tilde{q}_\mathrm{s})^\top \tilde{v}_\mathrm{s} < 0$ and for every well-defined and finite time interval $I_\mathrm{jump} \coloneqq (\tau_\mathrm{s}, \tau_\mathrm{r})$ the following properties: (i) $c(\tilde{q}(\tau)) \leq 0$, $\forall \tau \in I_\mathrm{jump}$, (ii) $n(\tilde{q}(\tau_\mathrm{r}))^\top \tilde{v}(\tau_\mathrm{r}) = 0$, and (iii) $c(\tilde{q}(\tau_\mathrm{r})) = 0$.*

In order to construct the *time-freezing system* we make several observations. First, the Filippov sliding motions are described by DAEs since the ODE $\dot{x} = \hat{f}_\mathrm{F}(x)$ has to fulfill the constraint $h(x) = 0$ (where $x = (q, v)$ and $\dot{q} = v$). Second, the inelastic restitution law (9d) is equal to the total time derivative of the constraint $c(q) = 0$, i.e., $\frac{\mathrm{d}}{\mathrm{d}t} c(q) = n(q)^\top v = 0$. We choose these functions as switching functions, i.e., $h_1(x) = n(q)^\top v$ and $h_2(x) = c(q)$. Third, the *switching manifold* $\Sigma \coloneqq \{x \mid h_1(x) = 0, h_2(x) = 0\}$ is in fact defined by the consistent initialization conditions (12) and therefore sliding motions of $\hat{f}_\mathrm{F}(x)$ evolve on Σ just as solutions of $\dot{x} = f_\mathrm{DAE}(x)$, the index reduced ODE corresponding to (11). Fourth, sliding motions enable us to consider switches between ODEs and DAEs of index 3. Fifth, exploiting the unused space $c(q) < 0$ and $n(q)^\top v < 0$ enables us to define an auxiliary ODE as in Definition 5 to get rid of the discontinuity in time. Sixth, by picking an appropriate ODE in $c(q) \leq 0$ and $n(q)^\top v \geq 0$ (as detailed later) we can ensure that for $x \in \Sigma$ the equation $\hat{f}_\mathrm{F}(x) = f_\mathrm{DAE}(x)$ holds, i.e., the sliding motion is the same as the solution of the DAE of index 3 after the state jump.

The reasoning above is summarized and depicted in a 2D projection in Figure 2. In the regions R_2 and R_4 we have the same smooth ODE, i.e., $f_2(\tilde{x}) = f_4(\tilde{x}) = f_\mathrm{ODE}(\tilde{x})$. In region R_1 the auxiliary ODE mimics the state jump, i.e., $f_1(\tilde{x}) = f_{\mathrm{A,n}}(\tilde{x})$. Region R_3 is equipped with the (possibly nonsmooth) vector field $f_3(\tilde{x}) = f_\mathrm{DF}(\tilde{x})$, denoted as *DAE-forming ODE*, which ensures that the sliding motion dynamics on Σ are the same as $f_\mathrm{DAE}(\tilde{x})$. Moreover, since in general $\nabla h_1(\tilde{x})^\top f_1(\tilde{x}) > 0$ at $x \in \Sigma$, the role of $f_3(\tilde{x})$ is also to stop the evolution of the trajectory in the space spanned by the columns of $\nabla h(\tilde{x})$ and to stay on Σ. Therefore, we request that $\nabla h_1(\tilde{x})^\top f_3(\tilde{x}) < 0$. Note that the solution trajectories never flow in R_3 and the system should not be initialized in this region.

Definition 6 (Time-Freezing PSS) *Let $\tau \in \mathbb{R}$ be the numerical time and $y(\tau) \coloneqq (\tilde{x}(\tau), t(\tau)) \in \mathbb{R}^{n_x+1}$ the differential states. The differential inclusion describing the time-evolution of the state vector $y(\tau)$*

$$y' \in F_\mathrm{TF}(y) \coloneqq \Big\{ \beta \tilde{f}_4(y) + (1-\beta)((1-\alpha)\tilde{f}_1(y) + \alpha \tilde{f}_3(y)) \mid \alpha \in \theta(\tilde{h}_1(x)),\ \beta \in \theta(\tilde{h}_2(x)) \Big\}, \tag{17}$$

with $\tilde{f}_1(y(\tau)) := \tilde{f}_{\mathrm{A,n}}(y(\tau)) = (f_{\mathrm{A,n}}(\tilde{x}(\tau)), 0)$, $\tilde{f}_2(y(\tau)) = \tilde{f}_4(y(\tau)) = \tilde{f}_{\mathrm{ODE}}(y(\tau)) := (f_{\mathrm{ODE}}(\tilde{x}(\tau)), 1)$, $\tilde{h}_i(y(\tau)) = h_i(\tilde{x}(\tau))$, $i = 1, 2$, *is denoted as the time-freezing system. It is assumed that appropriate dynamics* $f_{\mathrm{A,n}}(\tilde{x})$ *and* $\tilde{f}_3(y)$ *exist.*

The definition alone does not imply that the set of solutions of the time-freezing PSS is identical to the solution set of the CLS from Definition 4. To achieve this goal we must specify how to select appropriate auxiliary and DAE-forming ODEs. Finally, how to recover a solution of the original system (9) is described in Theorem 10. Note that equation (17) is slightly simpler than (8), since we have the same vector field in R_2 and R_4. Denote by $\tilde{\Sigma}_i := \{y \in \mathbb{R}^{n_x+1} \mid \tilde{h}_i(y) = 0\}$, $i = 1, 2$, the individual co-dimension one manifolds and by $\tilde{\Sigma} = \tilde{\Sigma}_1 \cap \tilde{\Sigma}_2$ their intersection. The next proposition provides a constructive way of selecting the auxiliary ODE from Definition 5 for any smooth scalar constraint $c(q) = 0$.

Proposition 7 (Auxiliary Dynamics) *Suppose that* $\tilde{x}(\tau_\mathrm{s}) = \tilde{x}_\mathrm{s} = (\tilde{q}_\mathrm{s}, \tilde{v}_\mathrm{s})$ *is given by* $c(\tilde{q}_\mathrm{s}) = 0$ *and* $n(\tilde{q}_\mathrm{s})^\top \tilde{v}_\mathrm{s} \leq 0$. *Then the ODE given by*

$$\tilde{x}'(\tau) = f_{\mathrm{A,n}}(\tilde{x}) = N(\tilde{q})\ (0, a_\mathrm{n}) \tag{18}$$

with $a_\mathrm{n} > 0$ *and* $N(\tilde{q}) := \begin{bmatrix} n(\tilde{q}) & \mathbf{0}_{n_q,1} \\ \mathbf{0}_{n_q,1} & G(\tilde{q})n(\tilde{q}) \end{bmatrix}$ *is an auxiliary dynamic system from Definition 5 with* $\tau_\mathrm{jump} = -\frac{n(\tilde{q}_\mathrm{s})^\top \tilde{v}_\mathrm{s}}{a_\mathrm{n} D(\tilde{q}_\mathrm{s})}$.

PROOF. Note that the state jump happens only along the constraint normal $n(\tilde{q}_\mathrm{s})$ at the *entry* point $\tilde{q}_\mathrm{s}$, with $c(\tilde{q}_\mathrm{s}) = 0$. Therefore, we can project the system on the normal, use a two-dimensional ODE and embed the result back. According to (18) we have $\tilde{q}'(\tau) = n(\tilde{q}) \cdot 0 = \mathbf{0}_{n_q,1}$, $\forall \tau \geq \tau_\mathrm{s}$, which implies $\tilde{q}(\tau) = \tilde{q}_\mathrm{s}$ and $c(\tilde{q}(\tau)) = 0$, $\forall \tau \geq \tau_\mathrm{s}$. This means also $N(\tilde{q}(\tau)) = N(\tilde{q}_\mathrm{s})$ and $G(\tilde{q}(\tau)) = G(\tilde{q}_\mathrm{s})$, $\forall \tau \geq \tau_\mathrm{s}$. Second, regard the dynamics of $\tilde{v}' = G(\tilde{q})n(\tilde{q})a_\mathrm{n} = G(\tilde{q}_\mathrm{s})n(\tilde{q}_\mathrm{s})a_\mathrm{n}$ and rewrite this equation in integral form. By multiply it from the left by $n(\tilde{q}_\mathrm{s})^\top$ we obtain:

$$n(\tilde{q}_\mathrm{s})^\top v(\tau) = n(\tilde{q}_\mathrm{s})^\top \tilde{v}_\mathrm{s} + n(\tilde{q}_\mathrm{s})^\top G(\tilde{q})n(\tilde{q}_\mathrm{s})a_\mathrm{n}(\tau - \tau_\mathrm{s}).$$

Since the first term on the r.h.s. is negative and the second strictly positive, we deduce that $n(\tilde{q}(\tau_\mathrm{r}))^\top \tilde{v}(\tau_\mathrm{r}) = 0$ and $c(\tilde{q}(\tau_\mathrm{r})) = 0$ with $\tau_\mathrm{jump} = \tau_\mathrm{r} - \tau_\mathrm{s} = -\frac{n(\tilde{q}_\mathrm{s})^\top \tilde{v}_\mathrm{s}}{a_\mathrm{n} D(\tilde{q}_\mathrm{s})}$. Hence, all conditions from Definition 5 are satisfied and the proof is complete. □

As discussed in Section 3 neither the Filippov nor the AP-extensions are guaranteed to have unique selections for some $y \in \tilde{\Sigma}$. Consequently, certain conditions have to hold for some chosen *selectors* $(\alpha^*(y), \beta^*(y)) \in [0, 1]^2$

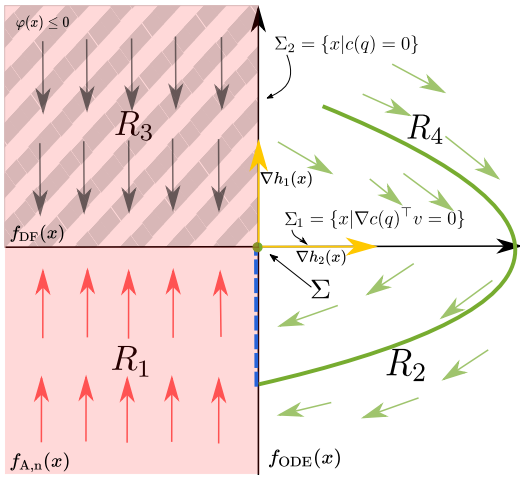

Fig. 2. Illustration of a phase plot of the time-frezing PSS from Definition 6. The red shaded area is the infeasible region of the CLS, where the trajectories of the auxiliary and DAE-forming dynamics flow. The green (solid) curve shows the resulting trajectory (a solution of the CLS) after discarding the time-frozen parts, cf. Theorem 10. The blue (dashed) curve shows a solution of the auxiliary ODE from Definition 5.

in order to ensure sliding modes of (17) for $y \in \tilde{\Sigma}$. The next lemma provides necessary conditions for this case. We introduce the following notation for the inner products: $\tilde{w}_{i,j}(y) := \nabla \tilde{h}_i(y)^\top \tilde{f}_j(y)$, $i \in \mathcal{I} = \{1, 2\}, j \in \mathcal{J} = \{1, 2, 3, 4\}$.

Lemma 8 (Feasible Selectors) *Suppose that* $y \in \tilde{\Sigma}$, *that we choose* $f_{\mathrm{A,n}}(\tilde{x})$ *from Proposition 7 and that for a chosen* $\tilde{f}_3(y)$ *in* (17) *we have* $\tilde{w}_{1,3} < 0, \tilde{w}_{2,3} = 0$. *If for some chosen selectors* $(\alpha^*(y), \beta^*(y)) \in [0, 1]^2$ *it holds* $F_{\mathrm{TF}}(y) \subset \mathcal{T}_{\tilde{\Sigma}}(y)$, *then*

$$0 = \tilde{w}_{1,1} + \beta^*(\tilde{w}_{1,2} - \tilde{w}_{1,1}) + \alpha^*(1 - \beta^*)(\tilde{w}_{1,3} - \tilde{w}_{1,1}). \tag{19}$$

PROOF. For $\tilde{f}_1 = (f_{\mathrm{A,n}}, 0)$ it is easy to verify that $\tilde{w}_{1,1} = a_\mathrm{n} > 0$ and $\tilde{w}_{2,1} = 0$. Note that $\tilde{w}_{1,2} = n(\tilde{q})^\top \tilde{v} = \tilde{h}_1(y)$ and with $y \in \tilde{\Sigma}$ it follows that $\tilde{w}_{1,2} = 0$. Requiring $F_{\mathrm{TF}}(y) \subset \mathcal{T}_{\tilde{\Sigma}}(y)$ is equivalent to the conditions $\nabla \tilde{h}_1(y)^\top F_{\mathrm{TF}}(y) = 0$ and $\nabla \tilde{h}_2(y)^\top F_{\mathrm{TF}}(y) = 0$. The first condition is in fact (19), the second holds under the given assumptions since $\tilde{w}_{2,j} = 0, j \in \mathcal{J}$. □

4.3 The DAE-Forming ODE and Contact Breaking

The goal of this subsection is to specify the DAE-forming dynamics in R_3 which enables: a) sliding on $\tilde{\Sigma}$ when the contact is persistent, b) leaving the sliding mode when the conditions for contact breaking are satisfied. According to Subsection 4.1, during persistent contact it holds that $\varphi(x) \leq 0$ and the CLS evolves according

to the DAE (11), which should be matched by the sliding mode of the time-freezing system defined by $F_{\mathrm{TF}}(y)$ for $y \in \tilde{\Sigma}$. Loosely speaking, a trajectory $y(\tau)$ stays on $\tilde{\Sigma}$, if all neighboring vector fields $\tilde{f}_1$ to $\tilde{f}_4$ point towards $\tilde{\Sigma}$. This property is called *attractivity* [12]. Therefore, the vector field in R_3 should be chosen such that attractivity holds. On the other hand, for $\varphi(x) > 0$ contact breaking should happen and $\tilde{\Sigma}$ should not be attractive anymore. Consequently, the vector field in R_3 must change such that the trajectory can leave into R_4 (where $\frac{\mathrm{d}^2}{\mathrm{d}\tau^2} c(q(\tau)) > 0$). This reveals the need for the switching function $h_3(x) = \varphi(x)$ which will govern the needed nonsmooth changes in R_3. At this point we remind the reader that $h_1(x) = n^\top(q)v$, $h_2(x) = c(q)$, that $\tilde{h}_i(y(\tau)) := h_i(\tilde{x}(\tau))$ and $\tilde{\Sigma}_i := \{y \in \mathbb{R}^{n_x+1} \mid \tilde{h}_i(y) = 0\}, i = 1, 2, 3$. Additionally, the manifold $\tilde{\Upsilon}$ is defined as $\tilde{\Upsilon} := \cap_{i=1}^{3} \tilde{\Sigma}_i$. Recall that $\tilde{f}_{\mathrm{ODE}}(y(\tau)) := (f_{\mathrm{ODE}}(\tilde{x}(\tau)), 1)$ and $\tilde{f}_{\mathrm{DAE}}(y(\tau)) := (f_{\mathrm{DAE}}(\tilde{x}(\tau)), 1)$. We introduce the compact notation $\gamma(y) \in \theta(\tilde{h}_3(y))$. The next proposition provides a DAE-forming ODE, where the aforementioned properties of the vector field in R_3 are given.

Proposition 9 (DAE-forming ODE) *Suppose that we chose $f_{\mathrm{A,n}}(\tilde{x})$ from Proposition 7 in the time-freezing system (17) and $y \in \tilde{\Sigma}$. Set the selectors to $\alpha^*(y) = \{0.5\}$, $\beta^*(y) = \{0\}$ and additionally let $\gamma^*(y) = \{0\}$ if $y \in \tilde{\Upsilon}$. Let $\tilde{f}_3(y)$ be equal to*

$$\begin{aligned} \tilde{f}_{\mathrm{DF}}(y) := (1 - \gamma(y))(2\tilde{f}_{\mathrm{DAE}}(y) - \tilde{f}_{\mathrm{A,n}}(y)) \\ + 2\gamma(y)\tilde{f}_{\mathrm{ODE}}(y), \end{aligned} \tag{20}$$

in Definition 6. The following statements hold:

(a) If $\varphi(x) \leq 0$, then $F_{\mathrm{TF}}(y) = \{\tilde{f}_{\mathrm{DAE}}(y)\} \subset \mathcal{T}_{\tilde{\Sigma}}(y)$, with $\tilde{w}_{1,3} < 0$ (sliding mode).

(b) If $\varphi(x) > 0$, then $F_{\mathrm{TF}}(y) = \{\tilde{f}_{\mathrm{ODE}}(y)\}$, with $\tilde{w}_{1,3} \geq 0$ (contact breaking).

PROOF. For (a), we have $\gamma(y) = 0$. We first verify that Lemma 8 holds for the chosen selectors. Under the given assumptions, it easy to verify that $\tilde{w}_{1,1} = a_{\mathrm{n}} > 0$ and $\tilde{w}_{2,1} = 0$. Moreover, evaluating $\tilde{w}_{1,3}$ we obtain $\tilde{w}_{1,3} = \nabla\tilde{h}_1(y)^\top(2\tilde{f}_{\mathrm{DAE}}(y) - \tilde{f}_{\mathrm{A,n}}(y)) = -a^{\mathrm{n}} < 0$. Similarly, we deduce that $\tilde{w}_{2,3} = 0$. Thus, all assumptions of Lemma 8 are satisfied and $\alpha^* = 0.5$ and $\beta^* = 0$ satisfy equation (19) for all $y \in \tilde{\Sigma}$. The relation $F_{\mathrm{TF}}(y) = \{\tilde{f}_{\mathrm{DAE}}(y)\}$ follows directly from evaluating the r.h.s of (17) with $(\alpha^*, \beta^*) = (0.5, 0)$. Note that, $y \in \tilde{\Upsilon}$, we have a sliding motion with $\gamma^* = 0$ and from direct evaluation, $F_{\mathrm{TF}}(y) = \{\tilde{f}_{\mathrm{DAE}}(y)\}$ still holds. For (b), we have $\gamma(y) = 1$ and by evaluating (17) (with $y \in \tilde{\Sigma}$) it follows that $F_{\mathrm{TF}}(y) = \{\tilde{f}_{\mathrm{ODE}}(y)\}$. Consequently, $\tilde{w}_{1,3} = \nabla\tilde{h}_1^\top \tilde{f}_{\mathrm{ODE}} = \varphi(y) > 0$. This completes the proof. □

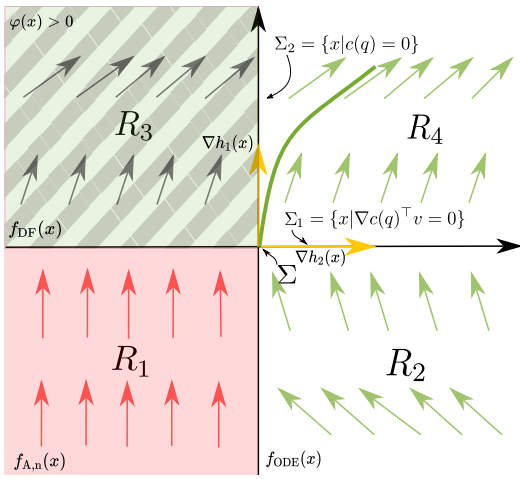

Fig. 3. The vector field in R_3 is changed compared to the vector field in R_3 in Figure 2, such that leaving of $\tilde{\Sigma}$ into R_4 is possible when $\psi(x) \geq 0$.

Case (a) of the last proposition is depicted in Figure 2. The vector fields point towards $\tilde{\Sigma}$ and a sliding mode happens. The vector fields for the contact breaking scenario (case (b) of the last proposition) are illustrated in Figure 3. Now a switch from $\tilde{f}_{\mathrm{DAE}}$ to $\tilde{f}_{\mathrm{ODE}}$ is possible. Note that in this case, for $y \in \tilde{\Sigma}$, we have $w_{1,j} > 0, w_{2,j} = 0, \forall j \in \mathcal{J}$. In consequence, $\tilde{\Sigma}$ is not attractive any more and y leaves $\tilde{\Sigma}$ and enters R_4. Moreover, for $y \in \tilde{\Upsilon}$, for our selection we obtain $F_{\mathrm{TF}}(y) = \{\tilde{f}_{\mathrm{ODE}}(y)\} \subset \mathcal{T}_{\tilde{\Upsilon}}(y)$ which corresponds to a sliding motion on a manifold of co-dimension 3, but with the desired vector field and $z(t) = 0$. Note that one can construct a DAE-forming ODE similar to (20) with different choices of $\alpha^*(y)$, $\beta^*(y)$ and $\gamma^*(y)$ which are not constant. This generalization complicates the expression of $\tilde{f}_{\mathrm{DF}}(y)$ without adding any advantages, since the constants next to $\tilde{f}_{\mathrm{DAE}}(y)$ and $\tilde{f}_{\mathrm{A,n}}(y)$ in (20) would be replaced by functions of y such that the equality (19) holds for all $y \in \tilde{\Sigma}$.

4.4 Solution Relationship

We formalize now how to recover the solution of the Initial Value Problem (IVP) corresponding to the CLS in 4 from the solution of the IVP corresponding to the time-freezing system from Definition 6.

Theorem 10 (Solution Relationship) *Regard the IVPs corresponding to: i) Definition 6 with a given $y_0 = (q_0, v_0, 0) \in \mathbb{R}^{n_x+1}$ and $c(\tilde{q}_0) \geq 0$ on a time interval $[0, \tau_{\mathrm{f}}]$, ii) Definition 4 with the initial value $x_0 = (q_0, v_0) \in \mathbb{R}^{n_x}$ on a time interval $[0, t_{\mathrm{f}}] := [0, t(\tau_{\mathrm{f}})]$, with $c(\tilde{q}(\tau_{\mathrm{f}})) \geq 0$ and $n(q(t_{\mathrm{f}}))^\top \tilde{v}(t_{\mathrm{f}}) \geq 0$. Suppose the following assumptions hold:*

(a) we choose $f_{\mathrm{A,n}}(\tilde{x})$ from Proposition 7 and $\tilde{f}_3(y)$ from

Proposition 9, in the DI from Definition 6,

(b) we have at most one time point $t_\mathrm{s} = t(\tau_\mathrm{s})$ *where* $c(q(t_s)) = 0$ *and* $n(q(t_\mathrm{s}))^\top v(t_\mathrm{s}^-) < 0$ *on the time interval* $[0, t_\mathrm{f}]$,

(c) for $y(\tau) \in \tilde{\Sigma}$ *we pick* $(\alpha^*, \beta^*) = (0.5, 0)$ *and for* $y(\tau) \in \tilde{\Upsilon}$ *we set additionally* $\gamma^* = 0$.

Then solutions of the two IVPs are related as follows:

(1) for $t \neq t_\mathrm{s}$*:*

$$x(t(\tau)) = Ry(\tau), \text{ with } R = \begin{bmatrix} \mathbf{1}_{n_x, n_x} & \mathbf{0}_{n_x,1} \end{bmatrix}, \tag{21a}$$

$$z(t(\tau)) = (1 - \beta(y(\tau)))(1 - \gamma(y(\tau)))f_z(\tilde{x}(\tau)), \tag{21b}$$

(2) for $t = t_\mathrm{s}$*:*

$$\lim_{\substack{\epsilon \to 0 \\ \epsilon > 0}} \int_{t_\mathrm{s}-\epsilon}^{t_\mathrm{s}+\epsilon} z(t)\mathrm{d}t = \int_{\tau_\mathrm{s}}^{\tau_\mathrm{r}} a_\mathrm{n}\mathrm{d}s. \tag{22}$$

PROOF. See Appendix A. □

Assumption (b), that we have at most one impact on $(0, t_\mathrm{f})$ is just for simplicity (and can be always satisfied by shortening the regarded time interval). Informally speaking, time-freezing enables one to make the state jump in "slow-motion". By plotting the state as function of physical time we make the "slow" transition "infinitely fast" and recover the discontinuity in time. More formally, this is encapsulated in (22), which shows that the integral of a Dirac impulse $z(t)$ is the same as the integral of the v-state of the auxiliary ODE over a finite time interval $I_\mathrm{jump} = [\tau_\mathrm{r}, \tau_\mathrm{s}]$ of nonzero length.

4.5 Auxiliary ODEs for Elastic Impacts

In contrast to inelastic impacts, with the auxiliary ODE for elastic impacts proposed in [22] one has $c(\tilde{q}) < 0$ during time-frozen periods $\tau \in (\tau_\mathrm{s}, \tau_\mathrm{r})$, cf. Figure 1 (top left plot). Consequently, $\tilde{q}(\tau) \neq q_\mathrm{s}$ holds for $\tau \in (\tau_\mathrm{s}, \tau_\mathrm{r})$, which makes the treatment of nonlinear constraints difficult (since the constraint normal $n(q)$ at the impact point q_s is needed, cf. Proposition 7). The depth of *diving* of $\tilde{q}(\tau)$ in the time-frozen period depends implicitly on the coefficient of restitution [22]. Treating multiple impacts with the old approach was only possible if the constraints are orthogonal in the kinetic metric [8,22]. However, if contact happens close to the corner where at least two constraint intersect at an obtuse angle, $\tilde{q}(\tau)$ might *dive* into the wrong region and make the reformulation invalid. This is resolved with the novel approach, since $c(\tilde{q}(\tau)) = 0$ for $\tau \in (\tau_\mathrm{s}, \tau_\mathrm{r})$.

We sketch the derivation of a novel auxiliary ODE for elastic impacts which overcomes the aforementioned drawbacks of [22]. To avoid *diving* into the infeasible region $c(\tilde{q}) < 0$ we introduce another state $p(\tau) \in \mathbb{R}$ which takes the role of $n(\tilde{q}(\tau))^\top \tilde{q}(\tau)$ and we *freeze* the evolution of $\tilde{q}(\tau)$ whenever $c(\tilde{q}) \leq 0$. The extended state space of the time-freezing system is given by $\hat{y}(\tau) = (y(\tau), p(\tau)) \in \mathbb{R}^{n_x+2}$ and let $\hat{x}(\tau) := (\tilde{q}(\tau), \tilde{v}(\tau), p(\tau))$. For $c(\tilde{q}) > 0$ we keep $y'(\tau) = \tilde{f}_\mathrm{ODE}(y)$ and set $p'(\tau) = 0$ and $p(0) = 0$, since $p(\tau)$ is not needed in this region. For $c(q) \leq 0$ the auxiliary dynamics mimics the state jump in $n(\tilde{q})^\top \tilde{v}$, but now in the space spanned by $[\nabla p \ \nabla(n^\top v)] \in \mathbb{R}^{n_q \times 2}$ instead of $[\nabla c(q) \ \nabla(n^\top v)] \in \mathbb{R}^{n_q \times 2}$. The state jump is emulated in $p \leq 0$ (and $c(\tilde{q}) \leq 0$). The evolution of $\tilde{q}(\tau)$ in this region is frozen, i.e., $\tilde{q}'(\tau) = 0$. In the space spanned by $[\nabla p \ \nabla(n^\top v)]$ we use 2D damped linear oscillator (as in [22]) to mimic the state jump. The result is then embedded back into $\mathbb{R}^{n_x+2}$. This behavior is modeled by the following vector field

$$f_{\mathrm{A}_-}(\hat{x}(\tau)) = \hat{N}(\tilde{q}) K \hat{N}(\tilde{q})^\top \hat{x}(\tau), \text{with}$$

$$\hat{N}(\tilde{q}) := \begin{bmatrix} N(\tilde{q}) & \mathbf{0}_{2n_q,1} \\ \mathbf{0}_{1,2} & 1 \end{bmatrix}, \ K = \begin{bmatrix} 0 & 0 & 0 \\ 0 & -c & -k \\ 0 & 0 & 1 \end{bmatrix}.$$

The term $\hat{N}(\tilde{q})^\top \hat{x}(\tau)$ projects $\hat{x}(\tau)$ into a three dimensional space. The first row of the matrix K *freezes* the evolution of $\tilde{q}(\tau)$ where the remaining rows model a damped second order linear oscillator, where with an appropriate choice of $k, c > 0$ we obtain $n(q_\mathrm{s})^\top v(\tau_\mathrm{r}) = -\epsilon n(q_\mathrm{s})^\top v(\tau_\mathrm{s})$, cf. [22, Section 3] for a detailed derivation. Similar to Proposition 7, the last multiplication by $\hat{N}(\tilde{q})$ embeds the result back into $\mathbb{R}^{n_x+1}$. It is left to define a vector field in the region $p > 0$ and $c(\tilde{q}) < 0$. The solution does not enter this region and the problem should not be initialized there. However, we define a vector field that points outwards of it, in case the trajectory enters this region due to numerical errors

$$f_{\mathrm{A}_+}(\hat{x}(\tau)) = \hat{N}(\tilde{q})(ae_3), a > 0.$$

Finally, with using $\eta \in \theta(p(\tau))$, we define the auxiliary

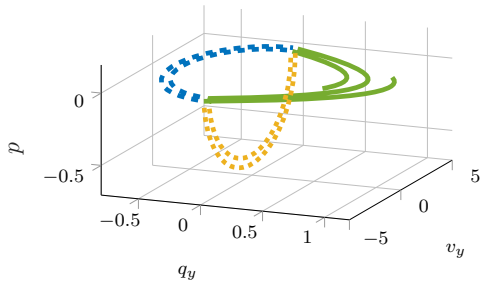

Fig. 4. The green (solid) and orange (dotted) curve show a solution to the elastic impact problem from Example 1 with the novel auxiliary ODE, and the blue (dashed) and green (solid) curve a solution with the auxiliary ODE form [22] (as in Figure 1 top left).

ODE

$$\hat{x}' = f_{\mathrm{A}}(\hat{x}) \coloneqq \eta f_{\mathrm{A}_+}(\hat{x}) + (1-\eta) f_{\mathrm{A}_-}(\hat{x}). \tag{23}$$

By extending the state space by $p(\tau)$ in Eq. (2) (cf. Subsection 2.2) and employing in the auxiliary ODE $\psi(\hat{x}) = f_{\mathrm{A}}(\hat{x}(\tau))$ the aforementioned difficulties are resolved. An illustration of a solution of the time-freezing system with the novel auxiliary ODE for the elastic case of Example 1 is depicted in Figure 4. The solution trajectory of the old auxiliary ODE [22] evolves in the $q_y - v_y$ plane (blue (dashed) curve) and $c(\tilde{q}) < 0$, $\tau \in (\tau_{\mathrm{s}}, \tau_{\mathrm{r}})$. In contrast to that, the solution trajectory of the novel ODE evolves in the $p - q_y$ plane (orange (dotted) curve) and it does not enter $c(\tilde{q}) < 0$. Therefore, $\tilde{q}(\tau) = q_{\mathrm{s}}$ holds for $\tau \in [\tau_{\mathrm{s}}, \tau_{\mathrm{r}}]$ and thus $\hat{N}(\tilde{q}(\tau)) = \hat{N}(q_{\mathrm{s}})$ results. Consequently, nonlinear constraints $c(q)$ can be treated naturally with the novel auxiliary ODE. Proving that (23) satisfies the conditions of [22, Assumption 1] follows similar lines as the proof of Proposition 7, hence solution equivalence holds due to [22, Theorem 1].

5 Computational Considerations

In this paper we focus on time-stepping methods for time-discretization [1,2,3,27]. These methods require solving a generalized equation at every time-step, have usually first-order accuracy [1], but preserve the nonsmoothness of the solution. Standard higher-order time-stepping integration schemes for smooth ODEs applied to DIs experience in general only first-order accuracy due to the lack of smoothness [1]. The lack of uniqueness in sliding motions requires some modifications of standard methods in order to solve OCP with time-freezing systems.

5.1 Time-Discretization

The implicit Euler discretization yields in many cases provably chattering-free sliding motions [2]. Therefore, we focus here on implicit schemes. Implicit discretizations for PSS transformed into DCS via the AP-extensions for gene regulatory networks are studied in [3]. We take here a similar approach for the time-freezing system, but with some modifications in order to handle nonuniqueness of sliding motions. We propose an optimization-based scheme, motivated by the fact that we have difficulties if more than one component of $\tilde{h}(y^{k+1})$ is zero (for a single component we obtain a unique Filippov vector field on a co-dimension 1 manifold).

We introduce the shorthand $\sigma \coloneqq (\alpha, \beta, \gamma)$. Every component of σ can be expressed via the the KKT conditions of (7) and we aggregate the Lagrange multipliers for the lower and upper bounds in (7) as $\lambda_0, \lambda_1 \in \mathbb{R}^3$, respectively. The *regularized* implicit Euler discretization of (17) with a step-size h solves at every time-step the following Mathematical Program with Complementarity Constraints (MPCC):

$$\begin{aligned}
\min_{y^{k+1},\, \sigma^{k+1}} \quad & \rho_{\mathrm{f}} \|\sigma^{k+1} - \sigma^*\|_2^2 && \text{(24a)}\\
\text{s.t.} \quad & y^{k+1} = y^k + h F_{\mathrm{TF}}(y^{k+1}, \sigma^{k+1}), && \text{(24b)}\\
& 0 = \tilde{h}(y^{k+1}) - \lambda_1^{k+1} + \lambda_0^{k+1}, && \text{(24c)}\\
& 0 \le \lambda_0^{k+1} \perp \sigma^{k+1} \ge 0, && \text{(24d)}\\
& 0 \le \lambda_1^{k+1} \perp \mathbf{1}_{3,1} - \sigma^{k+1} \ge 0, && \text{(24e)}
\end{aligned}$$

where y^{k+1} is the approximation of $y(\tau)$ at a time-step $\tau = (k+1)h$, y^k is the approximation for the previous time-step, σ^{k+1} and $\lambda_1^{k+1}, \lambda_0^{k+1}$ are discrete-time approximations of the selectors, and of the Lagrange multipliers, respectively. We denote this MPCC as the One Step Nonsmooth Problem (OSNP). The penalty parameter ρ_{f} is chosen to be not too large, in this paper we set $\rho_{\mathrm{f}} = 1$. Obviously, with $\rho_{\mathrm{f}} = 0$ we recover the standard implicit Euler scheme as a feasibility MPCC. Solution existence for a feasibility ONSP with $\rho_{\mathrm{f}} = 0$ in a similar form was proven in [3, Proposition 15].

Since in general the solution set of the OSNP in such a scenario is not a singleton, we must treat the case with multiple selectors appropriately. Note that if $\tilde{h}_i(y^{k+1}) \neq 0, i \in \mathcal{I}$, then the corresponding LP and the resulting complementarity conditions in (24) have single-valued solutions and the constraints of the MPCC (24) reduce to a standard implicit Euler step which has a unique solution. In this case, the objective of the MPCC (24) is just evaluated and has no influence on the solution. On the other hand, if more than one $\tilde{h}_i(y^{k+1}) = 0, i \in \mathcal{I}$, the constraints yield an underdetermined set of equations. Clearly, the optimal solution of the corresponding component of σ^{k+1} is equal to the matching component of σ^*. This effectively yields the desired selectors for sliding motions. Moreover, in all of our numerical experiments, we add additional algebraic variables and the corresponding constraints to *lift* the multi-affine selector terms in $F_{\mathrm{TF}}(y^{k+1}, \sigma^{k+1})$ such that the new algebraic variables enter the ODE linearly (e.g., $\alpha^{k+1}\beta^{k+1}$ is replaced by θ_1^{k+1}, and we add the constraint $\theta_1^{k+1} = \alpha^{k+1}\beta^{k+1}$, and so on) [4]. This greatly improves the convergence of this approach in practice.

To demonstrate the need of the regularization, we revisit Example 1, with $\epsilon = 0$, where we simulate the time-freezing system with the proposed scheme (24), both with $\rho_{\mathrm{f}} = 0$ and $\rho_{\mathrm{f}} = 1$. Consider a simulation of this system for $t \in [0, 2]$ for $q(0) = (0, 0)$ and $v(0) = (5, 0)$. Note that for this initial value we have $x(t) \in \Sigma, \forall t \in [0, 2]$. With $\rho_{\mathrm{f}} = 0$ we effectively calculate some feasible selectors σ^{k+1} without the guarantee that they are equal to σ^* as needed by Theorem 10. The blue (dashed) curves in the first two plots in Figure 5 show the obtained se-

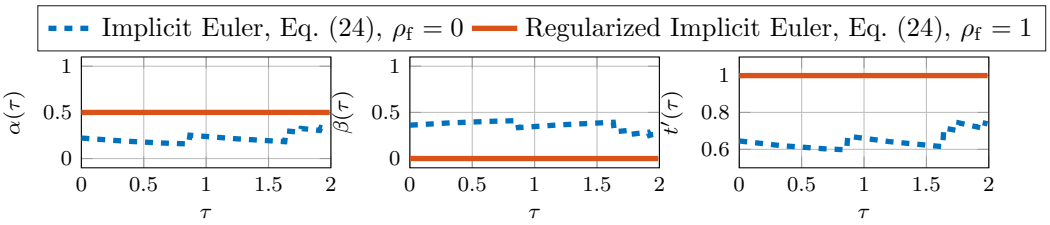

Fig. 5. Selectors and time derivative of the clock state calculated via a standard nonsmooth implicit Euler scheme and a regularized optimization-based scheme for Example 1.

lectors. Clearly, they differ from the needed values to ensure solution equivalence. The right plot shows that consequently the clock state derivative is $t'(\tau) \neq 1$. We repeat the experiment, but now with $\rho_f = 1$ were the objective term contributes to selecting the desired selectors. One can observe that during the whole simulation we obtain the needed selectors and the solution of the CLS can be reconstructed by means of Theorem 10.

5.2 Solving discretized OCP via homotopies for MPCCs

We take a simultaneous approach in direct optimal control [24, Chapter 8], that is we use the constraints of (24) as constraints of a discretized OCP and add its cost function to the objective of the OCP. In this paper we solve the MPCCs via a homotopy penalization approach. In the penalty reformulation an ℓ_1 or ℓ_∞ norm of the complementarity residual (i.e., the bilinear terms) is added to the objective and penalized by a positive weight ρ_{mpcc} [6,18,23]. Moreover, homotopy approaches help to avoid convergence to spurious local solutions [21,29]. An appealing property of such reformulation is: if ρ_{mpcc} is larger than a critical value, then the complementarity constraints are satisfied exactly at the solution [6,23]. This enables us to recover nonsmooth solutions by solving smooth NLPs. We solve a sequence of NLPs for different fixed values of the penalty parameter ρ_{mpcc} and update it via $\rho_{\text{mpcc}}^{k+1} = \kappa \rho_{\text{mpcc}}^{k}$ with k being the number of the problem in the sequence and $\kappa > 1$. All NLPs in this paper are solved with `IPOPT` [31] via its `CasADi` [5] interface.

6 Frictional Impact

If friction is present, state jumps caused by frictional impulses in the tangential directions must be considered as well. To model this case, the time-freezing reformulation from Sections 4 must be extended. The main assumption we make is that after an impact, the tangential velocities are zero, i.e., there is no slipping. This is a common modeling assumption in manipulation, walking and running in robotics [20,25]. A modified CLS with a single unilateral constraint with such tangential state jump law reads as:

$$\dot{v}(t) = f_{\text{v}}(q, v) + G(q)(n(q)z(t) + T(q)w(t)), \tag{25a}$$
$$\dot{q}(t) = v(t), \tag{25b}$$
$$0 \leq z(t) \perp c(q(t)) \geq 0, \tag{25c}$$
$$0 \leq w(t) \perp c(q(t))e_{m_w} \geq 0, \tag{25d}$$
$$0 = n(q(t_{\text{s}}))^\top v(t_{\text{s}}{}^+),\ 0 = T(q(t_{\text{s}}))^\top v(t_{\text{s}}{}^+), \quad \text{if } c(q(t_{\text{s}})) = 0 \text{ and } n(q(t_{\text{s}}))^\top v(t_{\text{s}}{}^-) < 0. \tag{25e}$$

The columns of the matrix $T(q) \in \mathbb{R}^{n_q \times m_w}$ span the tangent space of $c(q) = 0$ at the point of contact q, and $w(t) \in \mathbb{R}^{m_w}$ are the corresponding Lagrange multipliers. Note that $m_w = 1$ for planar impacts and $m_w = 2$ for 3D impacts. Compared to (9), in this formulation we have additional state jumps in the tangential directions, which are encoded by (25d) and the second equation in (25e). For the state jumps in the tangential directions the auxiliary ODEs can be assembled in the same manner for every column of $T(q)$. Hence, for ease of exposition we consider a $T(q)$ denoted as $t(q) \in \mathbb{R}^{n_q}$. Since the state jump can occur both for positive and negative $t(\tilde{q})^\top \tilde{v}$, the auxiliary ODE depends on the sign of $t(\tilde{q})^\top \tilde{v}$. In the virtue of Proposition 7 we define for $t(\tilde{q})^\top \tilde{v} < 0$, with a constant $a_{\text{t}} > 0$, the auxiliary ODE:

$$\tilde{x}' = f_{\text{A,t}}(\tilde{x}) := \begin{bmatrix} t(\tilde{q}) & \mathbf{0}_{n_q,1} \\ \mathbf{0}_{n_q,1} & G(\tilde{q})t(\tilde{q}) \end{bmatrix} \begin{bmatrix} 0 \\ a_{\text{t}} \end{bmatrix}. \tag{26}$$

The r.h.s. of the auxiliary ODE including the clock state is defined as $\tilde{f}_{\text{A,t}}(y) := (\tilde{f}_{\text{A,t}}(\tilde{x}), 0)$. To account for the sign of the tangential velocity we introduce another step function $\zeta(y) \in \theta(t(\tilde{q})^\top \tilde{v})$, with the desired selector $\zeta^* = 0.5$. The next function collects the auxiliary ODEs for the state jumps both in normal and tangential directions

$$\tilde{f}_{\text{jmp}}(y) := (1 - \alpha(y))\tilde{f}_{\text{A,n}}(y) + (1 - 2\zeta(y)))\tilde{f}_{\text{A,t}}(y).$$

The term $1 - 2\zeta(y) \in \text{sign}(t(\tilde{q})^\top \tilde{v})$ takes care of the sign of the tangential velocity and adapts the auxiliary ODE. Provided that consistent initialization holds, by index reduction we can find an explicit formula for the Lagrange multiplier $w(t)$ for the *no slipping* constraint $t(q)^\top v = 0$ and derive an ODE whose r.h.s is denoted as $f_{\text{DAE,f}}(x)$, which is equivalent to the post-impact DAE.

Similar to Proposition 9, we define a DAE-forming ODE for this case as

$$\tilde{f}_{\mathrm{DF,f}}(y) \coloneqq \frac{(1-\zeta(y))\zeta(y)}{\xi^*}\Big((1-\gamma(y))\tilde{f}_{\mathrm{DAE,f}}(y) + \gamma(y)\tilde{f}_{\mathrm{ODE}}(y)\Big) - (1-\gamma(y))\tilde{f}_{\mathrm{A,n}}(y).$$

The novelty compared to Proposition 9 is the term $(1-\zeta(y))\zeta(y)$ which makes sure that no sliding mode or contact breaking happen before the evolution of all auxiliary ODEs (i.e., state jumps) is finished. The role of $\gamma(y)$ is unchanged, it adapts the vector field such that either sliding mode or contact breaking happen. The constant $\xi^* = \zeta^*(1-\zeta^*)\alpha^*$ cancels the scaling of the nonzero selectors in sliding modes. Similar to (17), the time-frozen dynamics with frictional impact reads as

$$y' \in F_{\mathrm{TF,f}}(y) \coloneqq \Big\{\beta\tilde{f}_{\mathrm{ODE}}(y) + (1-\beta)\big(\tilde{f}_{\mathrm{jmp}}(y) + \alpha\tilde{f}_{\mathrm{DF,f}}(y)\big) \mid \alpha \in \theta(\tilde{h}_1(y),\ \beta \in \theta(\tilde{h}_2(y))\Big\}. \tag{27}$$

By direct evaluation of the r.h.s. for $y \in \tilde{\Sigma}$ with appropriate selectors it is straightforward to verify that $F_{\mathrm{TF,f}}(y) = \{\tilde{f}_{\mathrm{DAE,f}}(y)\}$ and in case of contact breaking $F_{\mathrm{TF,f}}(y) = \{\tilde{f}_{\mathrm{ODE}}(y)\}$. To further simplify this reformulation, we may assume that $t(\tilde{q})^\top\tilde{v} < n(\tilde{q})^\top\tilde{v}$ and that $a_{\mathrm{t}} \gg a_{\mathrm{n}}$. Hence, the tangential state jump is finished much faster then the jump in normal direction. According to Coulomb's law the tangential impulse is less than the friction coefficient times the normal contact impulse. Hence, it is unrealistic that for $t(\tilde{q})^\top\tilde{v} \gg n(\tilde{q})^\top\tilde{v}$ we do not have slip. These assumptions imply that we can drop the term $(1-\zeta(y))\zeta(y)$ in $\tilde{f}_{\mathrm{DF,f}}(y)$ (as $\tilde{x}$ reaches $t(\tilde{q})^\top\tilde{v} = 0$ always faster than $n(\tilde{q})^\top\tilde{v} = 0$). Additionally, we need just to adapt the constant such that $\xi^* = \alpha^*$.

7 Numerical Optimal Control of a Jumping Robot

We consider a hopping robot that has to jump over three holes to reach a desired target. Thereby an OCP formulation for synthesizing dynamics motions of the single-legged 2D robot *Capler* [11,16] is derived. The robot is described by four degrees of freedom $q = (x_{\mathrm{B}}, z_{\mathrm{B}}, \phi_{\mathrm{knee}}, \phi_{\mathrm{hip}})$. Here, $(x_{\mathrm{B}}, z_{\mathrm{B}})$ are the coordinates of the robot's base at the hip and ϕ_{knee}, ϕ_{hip} are the angles of the hip and knee, respectively, cf. [11, Figure 1]. It is actuated by two direct-drive motors at the hip and knee joints. The robot's dynamics are compactly described by the CLS

$$M(q)\dot{v} = f(x,u) + n(q)\lambda_{\mathrm{n}} + t(q)\lambda_{\mathrm{t}}, \tag{28a}$$
$$0 \le \lambda_{\mathrm{n}} \perp c(q) \ge 0, \tag{28b}$$
$$0 \le \lambda_{\mathrm{t}} \perp c(q) \ge 0, \tag{28c}$$
$$0 = [n(q(t_{\mathrm{s}}))\ t(q(t_{\mathrm{s}}))]^\top v(t_{\mathrm{s}}{}^+), \quad \text{if } 0 = c(q(t_{\mathrm{s}})) \text{and } n(q(t_{\mathrm{s}}))^\top v(t_{\mathrm{s}}{}^-) < 0, \tag{28d}$$

where $M(q)$ is the inertia matrix, λ_{n} the normal contract force and λ_{t} the friction force. The function $f(x,u)$ collects the gravitational, centrifugal and Coriolis forces. The torques of the two motors $u(t) = (u_{\mathrm{knee}}(t), u_{\mathrm{hip}}(t))$ are the control variables. The model fits into the form of the CLS (25). Detailed derivation of model equations and all parameters for the robot considered in this subsection can be found in [14, Appendix A].

Denote by $p_{\mathrm{foot}}(q) = (p_{\mathrm{foot},x}(q), p_{\mathrm{foot},z}(q))$ and $p_{\mathrm{knee}}(q) = (p_{\mathrm{knee},x}(q), p_{\mathrm{knee},z}(q))$ the kinematic position of the robot's foot and knee, respectively. As the constraint function in (28b) we take $c(q) = p_{\mathrm{foot},z}(q)$. The CLS is transformed into a time-freezing system according to (27) with the simplified friction model, as discussed in the previous section. For a planar robot we need just one tangent, i.e., $t(q) = \nabla_q p_{\mathrm{foot},x}(q)$. The auxiliary ODEs constants are $a_{\mathrm{n}} = 200$ and $a_{\mathrm{t}} = 600$.

Furthermore, we consider several constraints on kinematic quantities in the OCP formulation. To avoid unnatural and too extensive bending of the joints, we introduce the constraints: $-\frac{3\pi}{8} \le \phi_{\mathrm{hip}} \le \frac{3\pi}{8}$ and $-\frac{\pi}{2} \le \phi_{\mathrm{knee}} \le \frac{\pi}{2}$. The control variables should not lead to the base or the knee hitting the ground, therefore we require that $p_{\mathrm{knee}}(q) \ge 0$ and $z_{\mathrm{B}} \ge 0$. The upper and lower bound on both control torques are $u_{\mathrm{ub}} = 60$ and $u_{\mathrm{lb}} = -60$, respectively. The objective in our OCP in (29) is to minimize the integral of the squared control torques while the robots reaches a given target position $q_{\mathrm{target}} = (3, 0.4, 0, 0)$ starting from the initial position $q_0 = (0, 0.4, 0, 0)$ with zero velocity $v_0 = \mathbf{0}_{4,1}$. The initial value is $y_0 = (q_0, v_0, 0)$. The prediction horizon is $\tau_{\mathrm{f}} = 2.5$ s. To approximate Coulomb's friction law during contact, we use the explicit expressions for the Lagrange multipliers λ_{t} and λ_{n} (which can be obtained by index reduction) and impose the inequality constraint (with a friction coefficient $\mu = 0.8$)

$$\lambda_{\mathrm{t}}(q(t), v(t), u(t)) \le \mu\lambda_{\mathrm{n}}(q(t), v(t), u(t)).$$

On the way to the target, the robot has to overcome three holes in the ground. Instead of using very complicated expressions for $c(q)$ we model the holes as regions that the robot should not enter. This is achieved by concave constraints inside the OCP requiring that p_{foot} is outside of $n_e = 3$ ellipsoids:

$$\left(\frac{p_{\mathrm{foot},x} - x_{\mathrm{c},k}}{a_k}\right)^2 + \left(\frac{p_{\mathrm{foot},z} - z_{\mathrm{c},k}}{b_k}\right)^2 \ge 1, k = 1, \ldots, n_e.$$

By appropriately picking $a_k, b_k, x_{\mathrm{c},k}$ and $z_{\mathrm{c},k}$ the desired shapes are trivially selected. In our example, we pick $z_{\mathrm{c},k} = 0$, $a_k = 0.5$ (width of the hole), $b_k = 0.1$ (kept low, should not enforce unnecessarily high jumps), $k = 1, 2, 3$. For the centers of the holes we pick $x_{\mathrm{c},1} = 0.5$, $x_{\mathrm{c},2} = 1.5$, $x_{\mathrm{c},3} = 2.5$. We collect all path-constraints (on the kinematics, friction and for the holes) into the function $g_{\mathrm{ineq}}(y) \ge 0$.

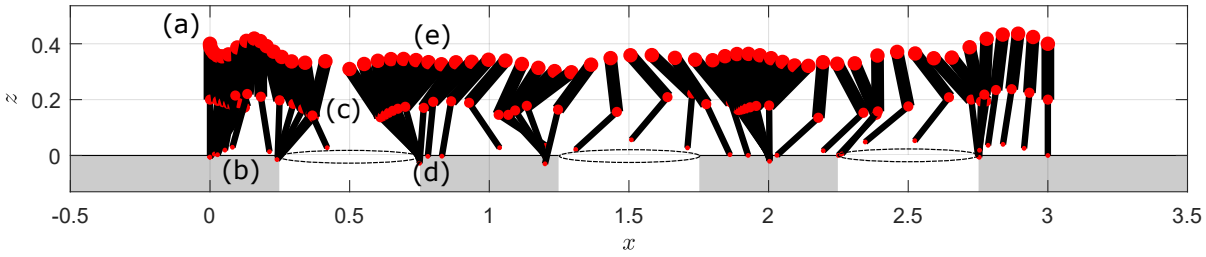

Fig. 6. Several frames of the solution of the discretization of the OCP (29). The dashed ellipsoids illustrate the hole constraints. The trajectory comprises all effects discussed in Sections 4 and 6: (a) initial sliding motion ($F_{\mathrm{TF}}(y) = \tilde{f}_{\mathrm{DAE,f}}(y)$); (b) contact breaking (switching from $\tilde{f}_{\mathrm{DAE,f}}(y)$ to $\tilde{f}_{\mathrm{ODE}}(y)$); (c) free flight ($\tilde{f}_{\mathrm{ODE}}(y)$); (d) state jump in normal and tangential direction (with $\tilde{f}_{\mathrm{A,n}}(y)$ and $\tilde{f}^{\mathrm{t}}(y)$); (e) switching from the auxiliary ODEs to the sliding motion (again to $\tilde{f}_{\mathrm{DAE,f}}(y)$).

Remark 11 *Note that the constraints $g_{\mathrm{ineq}}(q) \geq 0$ cannot become active if the corresponding normal velocity is nonzero (opposed to activating a constraint $c(q) \geq 0$), since no state jump law is associated with path-constraints in an OCP. This is one of the main differences between constraints which are part of the dynamics (equipped with a state jump law* (9d)*) and path-constraints in the OCP.*

The continuous-time OCP reads as:

$$\begin{aligned}
\min_{y(\cdot),u(\cdot)} \quad & \int_0^{\tau_{\mathrm{f}}} u(\tau)^2 \mathrm{d}\tau && \text{(29a)}\\
\text{s.t.} \quad & y(0) = y_0, && \text{(29b)}\\
& y'(\tau) \in F_{\mathrm{TF}}(y(\tau), u(\tau)), \tau \in [0, \tau_{\mathrm{f}}], && \text{(29c)}\\
& u_{\mathrm{lb}} e_2 \leq u(\tau) \leq u_{\mathrm{ub}} e_2, \tau \in [0, \tau_{\mathrm{f}}], && \text{(29d)}\\
& g_{\mathrm{ineq}}(y(\tau)) \geq 0, \tau \in [0, \tau_{\mathrm{f}}], && \text{(29e)}\\
& \tilde{q}(\tau_{\mathrm{f}}) = q_{\mathrm{target}}. && \text{(29f)}
\end{aligned}$$

The OCP is discretized with the regularized implicit Euler scheme from Section 5.1 (resulting in an additional cost term with $\rho_{\mathrm{f}} = 1$) with in total $N = 125$ discretization nodes resulting in $h = 0.02$ s. The discretized control inputs are set to be constant over the finite elements. A tiny fraction (since a_{n} and a_{t} are large) of the total numerical time is needed for the state jumps. If needed, a specific target for the physical time is easily reached with a time-transformation $s \geq 1$ and a terminal constraint $t(\tau_f) = \tau_f$), cf. Section 2.1 and [22, Section 5.2]. The resulting MPCC is solved as ℓ_∞ penalty-homotopy approach discussed in Section 5.2, with $\rho^0_{\mathrm{mpcc}} = 1, \kappa = 10$ and with 5 NLPs being solved in total. The complementarity constraints are satisfied exactly at the solution, hence we recover the optimal nonsmooth trajectories by solving a few smooth NLPs.

For the initialization of the differential states we take y_0 at every discretization node. All discrete-time control variables are initialized with zero. Hence, no information about the order, number or timing of the nonsmooth transitions and jumps is provided. Treating the contact dynamics directly in the OCP and thus directly discovering all nonsmooth transitions is in the robotics community called *contact implicit optimization* [11,30]. The results of the optimization are shown in Figure 6. All effects of the time-freezing reformulation discussed in Sections 4 to 6 can be observed in the solution. The approach finds an intuitive dynamic movement by solving only smooth NLPs, without providing any hints about the order and number of nonsmooth transitions. The drifts into the ground are due to inexact switch detection of the time-steeping scheme and are of order $O(h)$. The optimal torques are depicted in Figure 7. For the jumps over the holes large torques are applied, and the robot exploits its momentum to perform the smaller jumps in between holes with a smaller control effort.

8 Conclusion and Outlook

This paper introduced a novel time-freezing reformulation of dynamic systems with state jumps into piecewise smooth systems, thus reducing the level of nonsmoothnes significantly. While the elastic impact case was treated in [22], here we focus on the difficult case with inelastic impacts. We prove solution equivalence under mild conditions and derive constructive ways to select the auxiliary ODEs needed for solution equivalence. Moreover, we derive a novel auxiliary ODE for elastic impacts which overcomes some drawbacks of [22]. To the best of our knowledge, this the first reformulation which enables one to treat complementarity Lagrangian systems with inelastic impacts as Filippov systems. Furthermore, we derive a regularized implicit Euler scheme for discretization of time-freezing systems to alleviate the inherent nonuniqueness in sliding modes. The practicality of the discussed methods is demonstrated on an OCP considering an one-legged robot with frictional impact.

In future research we aim to investigate transformations of the time-freezing PSS into DCS where the multi-affine terms are avoided, e.g., with the reformulation used in [26]. Moreover, we believe that a more sophisticated penalty homotopy approach for the MPCCs [10,15] to-

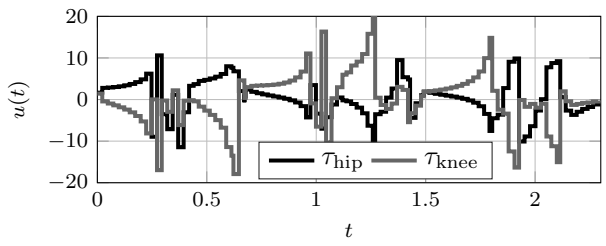

Fig. 7. The optimal control input $u(t)$ in physical time t obtained by solving the discretization of the OCP (29).

gether with a switch detecting time-discretization [7] will greatly improve the applicability of this reformulation.

Acknowledgements

We thank Jan Carius from ETH Zürich in Switzerland, for providing details for the *Capler* robot.

A Proof of Theorem 10

PROOF. A solution of the IVP given by (17) and y_0 is denoted as $y_{\text{sol}}(\tau; y_0)$ for some $\tau \in [0, \hat{\tau}]$. Similarly, for (9) and $x_0 = (q_0, v_0)$ for some $t(\tau) \in [0, t(\hat{\tau})]$ as $x_{\text{sol}}(t(\tau); x_0)$. Recall that $\tilde{h}_3(y(\tau)) = \varphi(\tilde{x}(\tau))$ (cf. eq. (15)) and denote by τ_{e} the time point with the following properties: $\tilde{h}_3(y(\tau_{\text{e}})) = 0$, $\tilde{h}_3(y(\tau)) =\leq 0$, $0 \leq \tau < \tau_{\text{e}}$ and $\tilde{h}_3(y(\tau)) \geq 0$, $\tau > \tau_{\text{e}}$. We must distinguish several possible cases, hence we split the proof in several parts.

Part I. Regard the case $c(\tilde{q}(\tau)) > 0, \tau \in [0, \hat{\tau}]$. This means $\beta(y(\tau)) = 1$, $y' = \tilde{f}_{\text{ODE}}(y), \tau \in [0, \hat{\tau}]$. Moreover, $t(\tau) = \int_0^\tau \mathrm{d}s = \tau$, set $\hat{\tau} = \tau_{\text{f}}$, consequently $t(\tau_{\text{f}}) = t_{\text{f}}$. We have that $Ry' = R\tilde{f}_{\text{ODE}}(y)$, is equivalent to $\tilde{x}' = f_{\text{ODE}}(\tilde{x})$. Since $[0, \tau_{\text{f}}] = [0, t_{\text{f}}]$, this ODE has the same solution as $\dot{x} = f_{\text{ODE}}(x)$, therefore relation (21a) holds for $t \in [0, t_{\text{f}}]$. This means $c(q(t)) > 0$ which implies for the CLS (9) $z(t) = 0$ for $t \in [0, t_{\text{f}}]$. Since $\beta(y(\tau)) = 1$ for $\tau \in [0, \tau_{\text{f}}]$ relation (21b) is also satisfied.

Part II. Regard the case $c(\tilde{q}(0)) = 0$ and $n(\tilde{q}(0))^\top \tilde{v}(0) = 0$, i.e., $y(0) \in \tilde{\Sigma}$. First, regard that $\tau_{\text{e}} > \tau_{\text{f}}$, this means that $f_z(\tilde{x}(\tau)) \geq 0$ (cf. (16a)), for $\tau \in [0, \tau_{\text{f}}]$. Due to assumptions (a), (c) and according to Proposition 9 we have $y' = \tilde{f}_{\text{DAE}}(y)$ for $\tau \in [0, \tau_{\text{f}}]$. Therefore, as in part I, $t'(\tau) = 1, \tau \in [0, \tau_{\text{f}}]$, thus $t(\tau_{\text{f}}) = \tau_{\text{f}} = t_{\text{f}}$. Under these conditions, we have $c(q(0)) = 0$, $n(q(0))^\top v(0) = 0$, $z(t) \geq 0$, $t \in [0, t_{\text{f}}]$. Consequently, the DCS (9) reduces to the DAE (11) which is equivalent to $\dot{x} = f_{\text{DAE}}(x)$ and similar to part I, we conclude that (21a) holds. In this setting we have, $\beta(y(\tau)) = \beta^* = 0, \tau \in [0, \tau_{\text{f}}]$. For $\tau \in [0, \tau_{\text{f}}]$ we have either: i) $\tilde{h}_3(y(\tau)) = 0$, with $\gamma(y(\tau)) = \gamma^* = 0$ and using (16a) we have $\tilde{f}_z(\tilde{x}(\tau)) = 0$ or, ii) $\tilde{h}_3(y(\tau_{\text{e}})) < 0$ (persistent contact), with $\gamma(y(\tau)) = 1$. Since (21a) holds and $f_z(\tilde{x}(\tau)) \geq 0$, and in the sliding mode $\beta^* = 0$ and $\gamma^* = 0$, we deduce that (21b) holds as well.

Part III. Now we consider the same scenario as in part II, i.e., $y_0 \in \tilde{\Sigma}$, but with $\tau_{\text{e}} \leq \tau_{\text{f}}$. Relations (21a) and (21b) hold for $\tau \in [0, \tau_{\text{e}})$ by the same arguments as in part II. For $\tau \geq \tau_{\text{e}}$, we have $\tilde{h}_3(y(\tau)) \geq 0$. If $\tilde{h}_3(y(\tau)) = 0$, for $\tau \in [\tau_{\text{e}}, \tau^*]$, with $\tau_{\text{e}} \leq \tau^* \leq \tau_{\text{f}}$, we have from (a) in Proposition 9 that $y' = \tilde{f}_{\text{DAE}}(y)$ and $\gamma(y) = \gamma^* = 0$. For this case, $y' = \tilde{f}_{\text{ODE}}$ and $\tilde{f}_z = 0$, and similarly for the DCS, $z(t) = 0$ and $\dot{x} = f_{\text{ODE}}$, thus (21a) and (21b) hold. On the other hand, if $\tilde{h}_3(y(\tau)) > 0$, for $\tau \in (\tau^*, \tau_{\text{f}}]$, due to (b) of Proposition 9, $\gamma(y) = 1$ and $y' = \tilde{f}_{\text{ODE}}(y)$. Since $(n(\tilde{q})^\top \tilde{v})^\top \tilde{f}_{\text{ODE}} > 0$ and $w_{1,j} > 0, w_{2,j} = 0, \forall j \in \mathcal{J}$, $y(\tau)$ leaves $\tilde{\Sigma}$ with $c(\tilde{q}(\tau)) > 0$, thus $\beta(y(\tau)) = 1$ and $y' = \tilde{f}_{\text{ODE}}(y)$, for $\tau > \tau^*$. Similarly, for the CLS (9) $\varphi(x) > 0$ implies $c(q(t)) > 0$ and $z(t) = 0$, for $t > t(\tau_{\text{e}})$ (cf. (14)). Therefore, for $\tau \in (\tau_{\text{e}}, \tau_{\text{f}}]$ we can apply the same arguments as for Part I and verify that (21a) and (21b) hold.

Part IV. This part regards the case of $\tau_{\text{s}} \in [0, \tau_{\text{f}}]$, i.e., $t_{\text{s}} \in [0, t_{\text{f}}]$. For $\tau \in [0, \tau_{\text{s}})$ and $t \in [0, t(\tau_{\text{s}}^-))$ we can apply Part I of the proof by simply setting $\hat{\tau} = \tau_{\text{s}}$ and deduce that (21a) and (21b) hold. For $\tau = \tau_{\text{s}}$ we have $c(\tilde{q}(\tau_{\text{s}})) = 0$ and $n(\tilde{q}(\tau_{\text{s}}))^\top \tilde{v}(\tau_{\text{s}}) < 0$. Consequently, $\alpha(y(\tau_{\text{s}})) = 0, \beta(y(\tau_{\text{s}})) = 0$ and $y' = \tilde{f}_{\text{A,n}}(y)$. The assumption $c(\tilde{q}(\tau_{\text{f}})) \geq 0$ and $n(q(t_{\text{f}}))^\top \tilde{v}(t_{\text{f}}) \geq 0$ ensures that $\alpha(y(\tau_{\text{f}})) > 0$, and thus that the time evolution of $y'(\tau) = f_{\text{A,n}}(\tau)$ is finished in $[\tau_{\text{s}}, \tau_{\text{f}}]$, i.e., $\tau_{\text{r}} \leq \tau_{\text{f}}$. From the proof of Proposition 7 we know that by construction $\tilde{q}(\tau) = \tilde{q}(\tau_{\text{s}}) =: \tilde{q}_{\text{s}}$, $\tau \in [\tau_{\text{s}}, \tau_{\text{r}}]$. Consequently, $c(\tilde{q}(\tau)) = 0$, $\tau \in [\tau_{\text{s}}, \tau_{\text{r}}]$. For $v(\tau)$, from (18) we have:

$$\tilde{v}(\tau_{\text{r}}) = \tilde{v}(\tau_{\text{s}}) + \int_{\tau_{\text{s}}}^{\tau_{\text{r}}} G(\tilde{q}(s)) n(\tilde{q}(s)) a_n \mathrm{d}s. \tag{A.1}$$

Multiplying both sides with $n(\tilde{q}_{\text{s}})^\top$ from the left and noting that $G(\tilde{q}(\tau))n(\tilde{q}(\tau))$ is constant since $\tilde{q}(\tau) = \tilde{q}_{\text{s}}$, $\tau \in [\tau_{\text{s}}, \tau_{\text{r}}]$, we have

$$\underbrace{n(\tilde{q}_{\text{s}})^\top v(\tau_{\text{r}})}_{=0} - n(\tilde{q}_{\text{s}})^\top v(\tau_{\text{s}}) = \underbrace{n(\tilde{q}_{\text{s}})^\top G(\tilde{q}_{\text{s}}) n(\tilde{q}_{\text{s}})}_{=D(\tilde{q}_{\text{s}})} \underbrace{\int_{\tau_{\text{s}}}^{\tau_{\text{r}}} a_n \mathrm{d}s}_{=:I_1},$$

$$I_1 = -\frac{n(\tilde{q}_{\text{s}})^\top v(\tau_{\text{s}})}{D(\tilde{q}_{\text{s}})}.$$

Next we look at the post-impact states of the CLS and compare to the time-freezing system. Since in CLSs with $r = 2$, $v(t)$ is a function of BV [28, Section 6.1], we have that $q(t) \in \mathcal{C}^0$ and thus $q(t_{\text{s}}^+) = q(t_{\text{s}}^-) = q(t_{\text{s}})$. Furthermore, notice that $q(t_{\text{s}}) = \tilde{q}_{\text{s}}$ which implies

$n(q(t_\mathrm{s}))^\top G(q(t_\mathrm{s}))n(q(t_\mathrm{s})) = D(\tilde{q}_\mathrm{s})$. Examining,

$$v(t_\mathrm{s}^+) = v(t_\mathrm{s}^-) + \underbrace{\lim_{\substack{\epsilon\to 0\\ \epsilon>0}} \int_{t_\mathrm{s}-\epsilon}^{t_\mathrm{s}+\epsilon} f_\mathrm{v}(q(s), v(s))\mathrm{d}s}_{=0} + \lim_{\substack{\epsilon\to 0\\ \epsilon>0}} \int_{t_\mathrm{s}-\epsilon}^{t_\mathrm{s}+\epsilon} G(q(s))n(q(s))z(s)\mathrm{d}s, \tag{A.2}$$

and multiplying both sides with $n(q_\mathrm{s})^\top$ from the left, introducing $I_2 \coloneqq \lim_{\substack{\epsilon\to 0\\ \epsilon>0}} \int_{t_\mathrm{s}-\epsilon}^{t_\mathrm{s}+\epsilon} z(s)\mathrm{d}s$, we conclude that

$$I_2 = -\frac{n(q(t_\mathrm{s}))^\top v(t_\mathrm{s}^-)}{D(\tilde{q}_\mathrm{s})} = I_1. \tag{A.3}$$

By comparing (A.1) and (A.2), due to the last relation we conclude that $\tilde{v}(\tau_\mathrm{r}) = v(t_\mathrm{s}^+) =: \tilde{v}_\mathrm{s}$. Furthermore, by Proposition 7 we have $c(q(\tau_\mathrm{r})) = 0$ and $n(\tilde{q}(\tau_\mathrm{r}))^\top \tilde{v}(\tau_\mathrm{r}) = 0$. Since $t'(\tau) = 0$ with $\tau \in [\tau_\mathrm{s}, \tau_\mathrm{r}]$, it follows that $t(\tau_\mathrm{r}) = t(\tau_\mathrm{s}) = t_s$. Consequently,

$$c(q(t_\mathrm{s})) = c(\tilde{q}(\tau_\mathrm{r})) = 0, \tag{A.4a}$$

$$n(q(t_\mathrm{s}))^\top v(t_\mathrm{s}^+) = n(\tilde{q}(\tau_\mathrm{r}))^\top \tilde{v}(\tau_\mathrm{r}) = 0. \tag{A.4b}$$

Let $y_\mathrm{s} \coloneqq (\tilde{q}_\mathrm{s}, \tilde{v}_\mathrm{s}, ts)$ and. Note that $y_\mathrm{sol}(\tau - \tau_\mathrm{r}, y_\mathrm{s}) = y(\tau, y_0)$ for $\tau \in [\tau_\mathrm{r}, \tau_\mathrm{f}]$. Likewise, $x_\mathrm{sol}(t - t_\mathrm{s}, x_\mathrm{s}) = x(t, x_0)$ for $t \in (t_\mathrm{s}, t_\mathrm{f}]$, with $x_\mathrm{s} = Ry_\mathrm{s}$. The two IVPs are initialized with the same initial conditions and the intervals $[\tau_\mathrm{s}, \tau_\mathrm{f}]$ and $(t_\mathrm{s}, t_\mathrm{f}]$ have the same length. For both DAEs $y' = \tilde{f}_\mathrm{DAE}(y)$ and $\dot{x} = f_\mathrm{DAE}(x)$ consistent initialization is ensured by (A.4). Therefore, by using the arguments of parts II or III (depending on τ_e), we deduce that (21a) and (21b) hold on $[\tau_\mathrm{r}, \tau_\mathrm{f}]$. Additionally, for $\tau \in (\tau_\mathrm{s}, \tau_\mathrm{r})$ we have $t = t_\mathrm{s}$. Note that equation (22) follows directly from (A.3).

Part V. Parts I-IV cover all relevant modes: evolution according to f_ODE (Part I), evolution on Σ according to f_DAE without leaving it (Part II) and with leaving it and continuing to evolve according to f_ODE (Part III), and the state jump (Part IV). To regard any other possible sequence of modes on $[0, \tau_\mathrm{f}]$, the time interval is simply split into sub-intervals with the different modes, and we apply subsequently the arguments from Parts I-IV to verify that (21a) and (21b) hold for $t \neq t_\mathrm{s}$ and (22) for $t = t_\mathrm{s}$. This completes the proof. □

References

[1] Vincent Acary and Bernard Brogliato. *Numerical Methods for Nonsmooth Dynamical Systems: Applications in Mechanics and Electronics*. Springer Science & Business Media, 2008.

[2] Vincent Acary and Bernard Brogliato. Implicit Euler numerical scheme and chattering-free implementation of sliding mode systems. *Systems & Control Letters*, 59(5):284–293, 2010.

[3] Vincent Acary, Hidde De Jong, and Bernard Brogliato. Numerical simulation of piecewise-linear models of gene regulatory networks using complementarity systems. *Physica D: Nonlinear Phenomena*, 269:103–119, 2014.

[4] Jan Albersmeyer and Moritz Diehl. The lifted Newton method and its application in optimization. *SIAM Journal on Optimization*, 20(3):1655–1684, 2010.

[5] Joel A. E. Andersson, Joris Gillis, Greg Horn, James B. Rawlings, and Moritz Diehl. CasADi: a software framework for nonlinear optimization and optimal control. *Mathematical Programming Computation*, 11(1):1–36, 2019.

[6] Mihai Anitescu, Paul Tseng, and Stephen J. Wright. Elastic-mode algorithms for mathematical programs with equilibrium constraints: global convergence and stationarity properties. *Mathematical Programming*, 110(2):337–371, 2007.

[7] Brian T. Baumrucker and Lorenz T. Biegler. MPEC strategies for optimization of a class of hybrid dynamic systems. *Journal of Process Control*, 19(8):1248–1256, 2009.

[8] Bernard Brogliato. *Nonsmooth Mechanics*. Springer International Publishing Switzerland, 2016. Third edition.

[9] Bernard Brogliato and Aneel Tanwani. Dynamical systems coupled with monotone set-valued operators: Formalisms, applications, well-posedness, and stability. *SIAM Review*, 62(1):3–129, 2020.

[10] Richard H. Byrd, Gabriel Lopez-Calva, and Jorge Nocedal. A line search exact penalty method using steering rules. *Mathematical Programming*, 133(1-2):39–73, 2012.

[11] Jan Carius, René Ranftl, Vladlen Koltun, and Marco Hutter. Trajectory optimization with implicit hard contacts. *IEEE Robotics and Automation Letters*, 3(4):3316–3323, 2018.

[12] Luca Dieci and Luciano Lopez. Sliding motion on discontinuity surfaces of high co-dimension. a construction for selecting a filippov vector field. *Numerische Mathematik*, 117(4):779–811, 2011.

[13] Aleksei Fedorovich Filippov. *Differential Equations with Discontinuous Righthand Sides*, volume 18. Springer Science & Business Media, Series: Mathematics and its Applications (MASS), 2013.

[14] Christian Gehring. Operational space control of single legged hopping. Master's thesis, Eidgenössische Technische Hochschule Zürich, Autonomous Systems Lab, 2011.

[15] Jonas Hall, Armin Nurkanović, Florian Messerer, and Moritz Diehl. A sequential convex programming approach to solving quadratic programs and optimal control problems with linear complementarity constraints. *IEEE Control Systems Letters*, 6:536–541, 2022.

[16] Jemin Hwangbo, Vassilios Tsounis, Hendrik Kolvenbach, and Marco Hutter. Cable-driven actuation for highly dynamic robotic systems. In *2018 IEEE/RSJ International Conference on Intelligent Robots and Systems (IROS)*, pages 8543–8550. IEEE, 2018.

[17] Jisu Kim, Hansung Cho, Artem Shamsuarov, Hyungbo Shim, and Jin H. Seo. State estimation strategy without jump detection for hybrid systems using gluing function. In *53rd IEEE International Conference on Decision and Control (CDC)*, pages 139–144. IEEE, 2014.

[18] Sven Leyffer, Gabriel López-Calva, and Jorge Nocedal. Interior methods for mathematical programs with complementarity constraints. *SIAM Journal on Optimization*, 17(1):52–77, 2006.

[19] Anna Machina and Arcady Ponosov. Filippov solutions in the analysis of piecewise linear models describing gene

regulatory networks. *Nonlinear Analysis: Theory, Methods & Applications*, 74(3):882–900, 2011.

[20] Katja Mombaur. Using optimization to create self-stable human-like running. *Robotica*, 27(3):321–330, 2009.

[21] Armin Nurkanović, Sebastian Albrecht, and Moritz Diehl. Limits of MPCC formulations in direct optimal control with nonsmooth differential equations. In *2020 European Control Conference (ECC)*, pages 2015–2020, 2020.

[22] Armin Nurkanović, Tommaso Sartor, Sebastian Albrecht, and Moritz Diehl. A time-freezing approach for numerical optimal control of nonsmooth differential equations with state jumps. *IEEE Control Systems Letters*, 5(2):439–444, 2021.

[23] Daniel Ralph and Stephen J. Wright. Some properties of regularization and penalization schemes for mpecs. *Optimization Methods and Software*, 19(5):527–556, 2004.

[24] James B. Rawlings, David Q. Mayne, and Moritz M. Diehl. *Model Predictive Control: Theory, Computation, and Design*. Nob Hill, 2nd edition, 2017.

[25] Gerrit Schultz and Katja Mombaur. Modeling and optimal control of human-like running. *IEEE/ASME Transactions on Mechatronics*, 15(5):783–792, 2009.

[26] David E. Stewart. A high accuracy method for solving ODEs with discontinuous right-hand side. *Numerische Mathematik*, 58(1):299–328, 1990.

[27] David E. Stewart. Rigid-body dynamics with friction and impact. *SIAM Review*, 42(1):3–39, 2000.

[28] David E. Stewart. *Dynamics with Inequalities: Impacts and Hard Constraints*, volume 59. SIAM, 2011.

[29] David E. Stewart and Mihai Anitescu. Optimal control of systems with discontinuous differential equations. *Numerische Mathematik*, 114(4):653–695, 2010.

[30] Yuval Tassa, Tom Erez, and Emanuel Todorov. Synthesis and stabilization of complex behaviors through online trajectory optimization. In *2012 IEEE/RSJ International Conference on Intelligent Robots and Systems (IROS)*, pages 4906–4913. IEEE, 2012.

[31] Andreas Wächter and Lorenz T. Biegler. On the implementation of an interior-point filter line-search algorithm for large-scale nonlinear programming. *Mathematical Programming*, 106(1):25–57, 2006.

[32] Viktor F. Zhuravlev. Equations of motion of mechanical systems with ideal one-sided constraints. *Prikladnaia Matematika i Mekhanika*, 42:781–788, 1978.